SMXL5 attenuates strigolactone signaling in *Arabidopsis thaliana*

Qingtian Li[1,2,3,*,C], Haiyang Yu[4,*], Wenwen Chang[5,6,*], Sunhyun Chang[1], Michael Guzmán[1], Lionel Faure[7], Eva-Sophie Wallner[8], Heqin Yan[2], Thomas Greb[8], Lei Wang[5], Ruifeng Yao[4,C], David C. Nelson[1C]

[1]Department of Botany and Plant Sciences, University of California, Riverside, CA 92521, United States of America

[2]Yazhouwan National Laboratory, Sanya 572025, China

[3]Yazhou Bay Seed Laboratory, Sanya 572025, China

[4]State Key Laboratory of Chemo/Biosensing and Chemometrics, Hunan Provincial Key Laboratory of Plant Functional Genomics and Developmental Regulation, College of Biology, Hunan University, Changsha 410082, China

[5]Key Laboratory of Seed Innovation, Center for Agricultural Resources Research, Institute of Genetics and Developmental Biology, Chinese Academy of Sciences, Shijiazhuang, Hebei 050021, China

[6]University of Chinese Academy of Sciences, Beijing 100049, China

[7]School of the Sciences, Biology Division, Texas Woman's University, Denton, TX 76204, United States of America

[8]Centre for Organismal Studies (COS), Heidelberg University, 69120 Heidelberg, Germany

*These authors contributed equally to this article

[C]Corresponding authors, David C. Nelson (david.nelson@ucr.edu); Qingtian Li (liqingtian@yzwlab.cn); Ruifeng Yao (ryao@hnu.edu.cn)

Running title: Attenuation of strigolactone signaling

The author(s) responsible for distribution of materials integral to the findings presented in this article is: Qingtian Li (liqingtian@yzwlab.cn)

ABSTRACT

Hormone-activated proteolysis is a recurring theme of plant hormone signaling mechanisms. In strigolactone signaling, the enzyme-receptor DWARF14 (D14) and an F-box protein, MORE AXILLARY GROWTH2 (MAX2), mark SUPPRESSOR OF MAX2 1-LIKE (SMXL) family proteins SMXL6, SMXL7, and SMXL8 for rapid degradation. Removal of these transcriptional corepressors initiates downstream growth responses. The homologous proteins SMXL3, SMXL4, and SMXL5, however, are resistant to MAX2-mediated degradation. We discovered that the *smxl4 smxl5* mutant has enhanced responses to strigolactone. *SMXL5* attenuates strigolactone signaling by interfering with AtD14-SMXL7 interactions. SMXL5 interacts with AtD14 and SMXL7, providing two possible ways to inhibit SMXL7 degradation. SMXL5 function is partially dependent on an EAR motif that typically mediates interactions with the TOPLESS family of transcriptional corepressors. However, we find that loss of the EAR motif reduces SMXL5-SMXL7 interactions and the attenuation of strigolactone signaling by SMXL5. We hypothesize that integration of SMXL5 into heteromeric SMXL complexes reduces the susceptibility of SMXL6/7/8 proteins to strigolactone-activated degradation, and that the EAR motif promotes the formation or stability of these complexes. This mechanism may provide a way to spatially or temporally fine-tune strigolactone signaling through the regulation of *SMXL5* expression or translation.

INTRODUCTION

Strigolactones (SLs) are plant hormones that control shoot branching/tillering, leaf development, root growth, anthocyanin biosynthesis, pathogen defense, and resilience to drought and phosphate starvation. SLs are also exuded from roots into soil, especially during low nitrogen or phosphorus availability. Rhizospheric SLs can stimulate symbiotic interactions with arbuscular mycorrhizal (AM) fungi or germination of root parasitic plants in the Orobanchaceae (Waters et al., 2017; Nelson, 2021).

SLs are perceived by the α/β-hydrolase DWARF14 (D14)/DECREASED APICAL DOMINANCE2 (DAD2), which has linked enzymatic and signal transduction activities (Hamiaux et al., 2012). D14 cleaves an enol-ether-linked methylbutenolide “D-ring” from SLs through nucleophilic attack, leading to covalent modification of one or more residues in the Ser-His-Asp catalytic triad (Yao et al., 2016; de Saint Germain et al., 2016; Chen and Shukla, 2022). D14 changes conformation during SL binding or hydrolysis, promoting its interaction with the F-box protein MORE AXILLARY GROWTH2 (MAX2)/DWARF3 (D3) and a subset of proteins in the SMAX1-LIKE (SMXL)/DWARF53 (D53) family. MAX2 is part of an SCF-type (Skp1-Cullin-F-box) E3 ubiquitin ligase complex (SCF^{MAX2}) that polyubiquitinates SMXL proteins, which are then rapidly degraded by the 26S proteasome (Jiang et al., 2013; Zhou et al., 2013; Wang et al., 2015; Yao et al., 2016). This initiates downstream SL responses.

In angiosperms, the *SMXL* gene family is composed of four major clades: *aSMAX1*, *SMXL78*, *SMXL39*, and *aSMXL4*. The *aSMAX1* and *SMXL78* clades form a super-clade, while the *SMXL39* and *aSMXL4* clades form another super-clade (Walker et al., 2019). One key distinction of SMXL39 and aSMXL4 proteins from other SMXL proteins is the lack of an “RGKT” (Arg-Gly-Lys-Thr), or P-loop, motif (Temmerman et al., 2022). Mutation of this motif renders aSMAX1 and SMXL78 proteins from multiple species resistant to SCF^{MAX2}-mediated polyubiquitination and degradation (Jiang et al., 2013; Zhou et al., 2013; Soundappan et al., 2015; Wang et al., 2015; Liang et al., 2016; Khosla et al., 2020a; Wang et al., 2020a; Zheng et al., 2020; Carbonnel et al., 2020).

SMXL clades are also distinguished by their functions and regulation. In *Arabidopsis thaliana*, *aSMAX1*, represented by *SMAX1* and *SMXL2*, regulates germination, photomorphogenesis, root and root hair development, and drought tolerance (Stanga et al., 2013; Stanga et al., 2016; Villaécija-Aguilar et al., 2019; Feng et al., 2022). *SMAX1* also controls primary root elongation and root hair development in *Lotus japonicus* (Carbonnel et al., 2020). An orthologous gene in rice (*Oryza sativa*), *OsSMAX1*, controls mesocotyl elongation in the dark and the capacity for root symbiotic interactions with AM fungi (Choi et al., 2020; Zheng et al., 2020). SMAX1 and SMXL2 proteins are primarily targeted for degradation by SCF^{MAX2} and KARRIKIN INSENSITIVE2 (KAI2), a homolog of D14. KAI2 mediates responses to karrikins (KARs), a class of butenolide compounds found in smoke, and a putative endogenous signal known as KAI2 ligand (Waters and Nelson, 2023). SMAX1 and SMXL2 can also be targeted by AtD14-SCF^{MAX2} when SL analogs are applied or during osmotic stress (Wang et al., 2020a; Li et al., 2022). By contrast, SMXL78 proteins, which are represented by SMXL6, SMXL7, and SMXL8 in Arabidopsis and D53 in rice, control SL-associated traits and are targeted by AtD14-SCF^{MAX2} after SL perception (Jiang et al., 2013; Zhou et al., 2013; Soundappan et al., 2015; Wang et al., 2015; Liang et al., 2016). In Arabidopsis, *SMXL39* is represented by *SMXL3*, and *aSMXL4* is represented by *SMXL4* and *SMXL5*. These genes regulate phloem development, and *SMXL4* also affects abiotic stress response, flowering time, and seed set (Yang et al., 2015; Wallner et al., 2017; Cho et al., 2018; Wallner et al., 2020; Yang et al., 2020). SMXL3, SMXL4, and SMXL5 proteins are resistant to degradation after treatment with *rac*-GR24, a racemic mixture of a synthetic SL analog, $GR24^{5DS}$, and its enantiomer, $GR24^{ent\text{-}5DS}$, that activates both AtD14 and KAI2 (Scaffidi et al., 2014; Wallner et al., 2017). Putatively, SMXL3/4/5 stability is a consequence of the absent RGKT motif.

SMXL proteins are distantly related to ClpB-type AAA+ proteins, which form hexameric complexes and function as molecular chaperones (Stanga et al., 2013; Temmerman et al., 2022). SMXL4, at least, retains weak ATPase activity (Yang et al., 2015). SMXL proteins are putatively transcriptional regulators, however. Like Aux/IAA proteins in auxin signaling and JAZ proteins in jasmonate signaling, SMXL proteins have a conserved

ethylene responsive element binding factor-associated amphiphilic repression (EAR) domain (Blázquez et al., 2020). In plants, EAR motifs are bound by TOPLESS (TPL) and TOPLESS-RELATED (TPR), members of the Groucho/Tup1 family of transcriptional corepressors in eukaryotes. TPL/TPR proteins participate in many signaling pathways in plants, repressing transcriptional activity via recruitment of histone deacetylases, interactions with the Mediator complex, and/or binding histone proteins (Leydon et al., 2021; Plant et al., 2021). SMXL proteins interact with TPL/TPR, and the EAR motif is important for many developmental functions of SMXL7 (Jiang et al., 2013; Soundappan et al., 2015; Wang et al., 2015; Liang et al., 2016). In association with TPL/TPR, D53 and SMXL6/7/8 regulate specific gene targets through interaction with transcription factors such as SQUAMOSA PROMOTER BINDING PROTEIN-LIKE (SPL) proteins and BRI1-EMS SUPPRESSOR1 (BES1)/BRASSINAZOLE-RESISTANT 1 (BZR1), but also by binding DNA directly (Liu et al., 2017; Song et al., 2017; Fang et al., 2020; Xie et al., 2020; Hu et al., 2020; Wang et al., 2020b; Sun et al., 2021).

Despite their homology, KAR/KL and SL pathways mostly have different functions in plant development. Their unique roles could be a consequence of specific expression patterns for the components of each pathway and/or regulation of different transcriptional networks by SMXL proteins. Promoter-swapping experiments have demonstrated that *KAI2* and *AtD14* are not interchangeable in Arabidopsis, putatively because of different preferences of the receptors for ligands and SMXL protein targets (Waters et al., 2015). However, it remains possible that SMXL proteins have interchangeable functions. Overlapping regulation of some downstream genes by SMXL proteins has been suggested in rice (Zheng et al., 2020). Furthermore, *SMAX1-YFP* can rescue the short primary root phenotype of Arabidopsis *smxl4,5* seedlings when expressed under control of a *SMXL5* promoter. Rescue is abolished by application of *rac*-GR24, which stimulates the rapid degradation of SMAX1-YFP (Wallner et al., 2017). This observation led us to investigate the extent to which SCF^{MAX2}-targeted and SCF^{MAX2}-resistant SMXL proteins can replace each other. Unexpectedly, we discovered that the *aSMXL4* clade attenuates SL signaling.

RESULTS

Strigolactone responses are enhanced in the *smxl4,5* mutant

We tested whether misexpression of *SMXL5* could compensate for genetic deficiencies in other *SMXL* clades in *Arabidopsis thaliana*. A *SMXL5-YFP* translational fusion expressed under the control of a *SMAX1* promoter (*pSMAX1:SMXL5-YFP*) did not rescue the short hypocotyl phenotype of *smax1 smxl2* seedlings, but *SMAX1-GFP* did (Figure 1A). Neither did *SMXL5-YFP* expressed under the control of a *SMXL7* promoter (*pSMXL7:SMXL5-YFP*) affect the reduced shoot branching or reduced leaf dimension phenotypes of the *smxl6,7,8* triple mutant (Figure 1B-1D). In contrast, *SMXL7-GFP* rescued *smxl6,7,8*. It is possible that *SMXL5-YFP* did not rescue *smax1 smxl2* or *smxl6,7,8* because the abundance of *SMXL5-YFP* transcripts in the two sets of transgenic lines was not quite as high as native *SMAX1* or *SMXL7* (Supplemental Figure 1A-1C). However, this does not necessarily mean that SMXL5-YFP had lower protein abundance than SMAX1 or SMXL7, as SMXL5 is not subject to MAX2-dependent degradation. Therefore, we currently find no evidence that *SMXL5* can replace *SMAX1*/*SMXL2* or *SMXL6*/*7*/*8* in Arabidopsis.

We then tested whether *SMXL7* misexpression can rescue genetic deficiencies in the *SMXL3/4/5* super-clade, or whether this is a *SMAX1*-specific effect. Expression of *SMXL7-GFP* under control of a *SMXL5* promoter (*pSMXL5:SMXL7-GFP*) did not recover growth of the *smxl3,4,5* triple mutant, which is seedling lethal (Wallner et al., 2017) (Supplemental Figure 2A). However, *pSMXL5:SMXL7-GFP* improved the growth of *smxl3 smxl4* plants that were heterozygous for *smxl5*, suggesting SMXL7 may partially compensate for reduced SMXL3/4/5 abundance (Supplemental Figure 2A). *pSMXL5:SMXL7-GFP* also rescued the short primary root and increased anthocyanin phenotypes of *smxl4,5* double mutant seedlings similarly to *pSMXL5:SMXL5-YFP* and *pSMXL5:SMAX1-YFP* (Figure 2A, Supplemental Figure 2B and 2C).

It was previously shown that *rac*-GR24 inhibits the rescue of *smxl4,5* root elongation by *pSMXL5:SMAX1-YFP*, which is putatively a consequence of the rapid *rac*-GR24-induced degradation of SMAX1-YFP protein (Wallner et al., 2017). However, because *rac*-GR24

activates both AtD14 and KAI2, and both receptors can work with SCF^{MAX2} to target SMAX1 for degradation, it is ambiguous which pathway(s) was affecting root growth. We investigated whether similar responses occur in *pSMXL5:SMXL7-GFP smxl4,5* lines. As reported for SMAX1-YFP, we found that SMXL7-GFP recovered *smxl4,5* root elongation and was degraded within 5 minutes of treatment with *rac*-GR24 (Figure 2A; Supplemental Figure 3A). We then examined seedling growth responses to AtD14- and KAI2-specific agonists, $GR24^{5DS}$ and KAR_2, respectively (Figure 2A; Supplemental Figure 4). Root elongation of wild-type (Col-0) and *pSMXL5:SMXL5-YFP smxl4,5* seedlings was weakly inhibited by 5 μM $GR24^{5DS}$, but was not significantly affected by 2 μM or 5 μM KAR_2. In contrast, *pSMXL5:SMXL7-GFP* and *pSMXL5:SMAX1-YFP smxl4,5* root elongation was strongly inhibited by $GR24^{5DS}$ treatment, presumably due to AtD14 activity. KAR_2 only inhibited the root growth of *SMAX1-YFP smxl4,5* seedlings, consistent with KAI2-SCF^{MAX2} activity. Unexpectedly, we noticed that *smxl4,5* roots were more sensitive to $GR24^{5DS}$ than Col-0, but were unaffected by KAR_2. This raised the possibility that SL signaling is more easily activated in *smxl4,5*.

To investigate whether *SMXL3/4/5* genes attenuate SL signaling, we examined the axillary bud outgrowth phenotypes of mutants in this clade. Rosette primary branch numbers of *smxl3*, *smxl4*, and *smxl5* single mutants were not different from Col-0 (Figure 2B and 2C). However, *smxl4,5* plants had fewer rosette branches. Branching was normal in *smxl3,4* and *smxl3,5*, although these double mutants have root elongation defects that are similar to *smxl4,5* (Wallner et al., 2017). These observations suggest that *SMXL4* and *SMXL5* promote shoot branching redundantly. Supporting this idea, overexpressing *SMXL5-YFP* with a *35S* promoter caused an increase in axillary branching (Supplemental Figure 5).

While the reduced shoot branching of *smxl4,5* could indicate a hypersensitive response to SL, alternatively it could have a SL-independent cause. To distinguish between these possibilities, we tested epistatic interactions between *smxl4,5* and the SL-insensitive mutants *Atd14* and *max2* (Figure 2B and 2C). Branching of *Atd14 smxl4,5* and *max2 smxl4,5* was not different from *Atd14* and *max2*, respectively, suggesting that the effect

of *smxl4,5* on shoot branching requires SL signaling. One way a hypersensitive SL response could occur is if *smxl4,5* has reduced abundance of SMXL6/7/8 proteins. Supporting this idea, *pSMXL5:SMXL7-GFP* rescued *smxl4,5* branching, but *pSMXL5:SMAX1-YFP* did not (Figure 2B and 2C). We also observed that combining *smxl6,7,8* mutations with *smxl4,5* had severe effects on growth that were reminiscent of *smxl3,4,5* (Supplemental Figure 6).

To better understand the *smxl4,5* branching phenotype, we examined the expression of *BRANCHED1* (*BRC1*), a transcriptional regulator that inhibits axillary bud outgrowth. *BRC1* expression is induced by SL and suppressed by *SMXL6*/*7*/*8* (Aguilar-Martínez et al., 2007; Wang et al., 2020b). In axillary buds, *BRC1* expression was increased in *smxl4,5* relative to Col-0, consistent with the reduced branching phenotype of the double mutant (Figure 2D). Upregulation of *BRC1* in *smxl4,5* buds was dependent on *MAX2*. In contrast, the *smxl6,7,8* triple mutant, which also showed increased *BRC1* transcript abundance in buds, was epistatic to *max2* (Figure 2D). We also found that *SMXL7* transcripts were more abundant in *smxl4,5* buds than Col-0 (Figure 2E). This may be a consequence of negative feedback regulation of SL signaling; i.e., high SL signaling induces *SMXL6/7/8* expression, while low SL signaling represses it (Wang et al., 2020b). Again, this phenotype was *MAX2*-dependent. In seedlings, $GR24^{5DS}$ application elicited a stronger increase of *BRC1* transcripts in *smxl4*,*5* compared with Col-0 (Figure 2F). This phenotype was rescued by *pSMXL5:SMXL5-YFP*. In contrast, *BRC1* expression in *Atd14 smxl4*,*5* or *max2 smxl4*,*5* seedlings was not affected by $GR24^{5DS}$, indicating the effect of *smxl4,5* on *BRC1* expression requires SL signaling. Altogether, these results provide evidence that SL signaling is enhanced in *smxl4,5*.

We then used a transient coexpression assay to test whether *SMXL5* affects the activity of a *BRC1* transcriptional reporter in the presence of SMXL7-FLAG fusion protein. In wild-type *Nicotiana benthamiana* leaves, luciferase activity from *pBRC1:LUC* increased approximately 2-fold after a 3 h treatment with $GR24^{5DS}$ (Figure 2G). Coexpression of *35S*:*SMXL5-YFP* reduced the luciferase signal before treatment and blocked its induction by $GR24^{5DS}$. At the same time, we observed increased SMXL7-FLAG protein levels in

leaves that were co-transformed with *35S:SMXL5-YFP* (Supplemental Figure 7). In a SL-insensitive *N. benthamiana* double mutant, *Nbd14a,b* (White et al., 2021), GR24^{5DS} did not induce luciferase activity and *SMXL5* coexpression had no observable effect. This suggested that *SMXL5* inhibits the AtD14-mediated transcriptional response of *BRC1* to SL.

SMXL4 and SMXL5 inhibit strigolactone-induced degradation of SMXL7 and AtD14

These results led us to hypothesize that *SMXL4* and *SMXL5* reduce SL-induced targeting of SMXL6/7/8 by AtD14-SCF^{MAX2}. To test this idea, we asked whether *SMXL4* and *SMXL5* affect SL-induced degradation of a SMXL7-GFP fusion protein in Arabidopsis seedlings. We observed a significant decline in SMXL7-GFP abundance after five minutes of GR24^{5DS} treatment in *smxl4,5* seedlings but not in Col-0 or *max2 smxl4,*5 (Figure 3A). Over a longer time-course, SMXL7-GFP declined faster after GR24^{5DS} treatment in *smxl4,5* compared to Col-0, and was relatively stable in *max2 smxl4,5* (Supplemental Figure 8). As a complementary test, we transiently coexpressed a *SMXL7* ratiometric reporter (Khosla et al., 2020a), *AtD14* or a catalytically inactive *Atd14^{S97A}* mutant, and *SMXL5* or an empty vector in *Nbd14a,b* leaves (Figure 3B). In the presence of *AtD14*, the ratio of fluorescence from a SMXL7-mScarlet-I reporter protein relative to a co-transcribed Venus reference protein declined 1.5-fold within 2 h of treatment with GR24^{5DS}. Supporting the hypothesis, when *SMXL5* was coexpressed, SMXL7 reporter levels were not reduced after GR24^{5DS} treatment. This was similar to what was observed in *Atd14^{S97A}* negative controls.

Like SMXL7, AtD14 is degraded after SL perception, but more slowly (Chevalier et al., 2014). We tested whether *SMXL4* and *SMXL5* affect the SL-induced degradation of AtD14. AtD14-CFP declined more quickly after GR24^{5DS} treatment in *smxl4,5* seedlings than in Col-0, but AtD14-CFP remained stable in *max2 smxl4,5* (Figure 3C; Supplemental Figure 8B). Consistent with this result, coexpression of *SMXL5* slowed the decline of an AtD14 ratiometric reporter (White et al., 2021) in *Nbd14a,b* leaves after GR24^{5DS} treatment (Figure 3D). The abundance of Atd14^{S97A} reporter protein was not affected by GR24^{5DS}. We conclude that *SMXL4* and *SMXL5* attenuate SL signaling.

SMXL5 inhibits interactions between AtD14 and SMXL7

This raised the question of how attenuation occurs. We hypothesized that SMXL4 and SMXL5 may reduce SL signaling by inhibiting interactions between AtD14-SCF^{MAX2} and SMXL6/7/8. We used a yeast three-hybrid assay to investigate whether SMXL5 interferes with AtD14-SMXL7 and/or AtD14-MAX2 interactions. In this assay, a conditional promoter (P_{MET25}) drove expression of *SMXL5* in the absence of methionine. We found that *rac*-GR24-induced interactions between AtD14 and SMXL7 were attenuated when P_{MET25}*:SMXL5* was induced in methionine dropout media, and restored by the addition of methionine (Figure 4A). In contrast, *rac*-GR24-induced interactions between AtD14 and ASK1-MAX2, a fusion of Arabidopsis Skp1 (part of the E3 ubiquitin ligase complex) and MAX2, were not affected by the induction of *SMXL5*. This suggested that SMXL5 inhibits AtD14-SMXL7 interactions specifically.

To validate this conclusion, we performed a split-luciferase complementation assay between AtD14 and SMXL7 in *N. benthamiana* leaves. Luciferase activity increased after a 1 h treatment with GR24^{5DS}, consistent with SL-stimulated interactions between cLUC-AtD14 and SMXL7-nLUC (Figure 4B). When *SMXL5* was coexpressed, however, there was a significant reduction in luciferase activity in both the absence and presence of GR24^{5DS}, suggesting that AtD14-SMXL7 interactions were inhibited by SMXL5. We also used a co-immunoprecipitation assay to test whether SMXL5 affected interactions between AtD14 and SMXL7 in Arabidopsis (Figure 4C). Co-immunoprecipitation of FLAG-tagged AtD14 protein by HA-tagged SMXL7 was reduced in protoplasts derived from *35S:SMXL5-YFP* transgenic plants compared to wild-type. Nonetheless, addition of GR24^{4DO}, another AtD14-specific SL analog (Wang et al., 2020b), enhanced the interaction of FLAG-AtD14 and HA-SMXL7 in both genetic backgrounds.

We hypothesized two ways that SMXL5 may interfere with SL-induced AtD14-SMXL7 interactions, which trigger SMXL7 polyubiquitination and proteosomal degradation (Figure 5A). First, SMXL5 might bind AtD14, preventing its association with SMXL7 through sequestration (Figure 5B). Arguing against this, prior research showed that GFP-

SMXL5 has very little or no interaction with HA-tagged AtD14 in co-immunoprecipitation assays compared to GFP-SMXL2 and GFP-SMXL6 (Wang et al., 2020a). However, we found evidence in yeast two-hybrid assays that SMXL5 can interact with AtD14 in the presence of $GR24^{5DS}$, although less well than SMXL7 (Figure 6A). SMXL5 did not interact with the inactive $Atd14^{S97A}$ mutant protein. Similarly, in split-luciferase complementation assays in *N. benthamiana*, $GR24^{5DS}$ induced an interaction between SMXL5-nLUC and cLUC-AtD14, but not cLUC-$Atd14^{S97A}$ (Figure 6B). Finally, in pull-down experiments with recombinant proteins we found that GST-SMXL5 interacts with His-GB1-AtD14, but not His-GB1-$Atd14^{S97A}$, in the presence of *rac*-GR24 (Figure 6C). Therefore, we conclude that AtD14-SMXL5 interactions can occur, although prior work suggests that these are probably weaker than AtD14-SMXL7 interactions (Wang et al., 2020a).

Our second hypothesis was that SMXL5, which is resistant to SCF^{MAX2}-induced degradation, may interact with and protect SMXL7 (Figure 5C). Support for SMXL-SMXL protein-protein interactions comes from the homology of SMXL proteins to hexameric ClpB ATPases, bimolecular fluorescence complementation and yeast two-hybrid assays, and the observation that hexameric GFP-D53 complexes form *in vitro* (Stanga et al., 2013; Ma et al., 2017; Khosla et al., 2020a). The possibility of protein-protein interactions between members of different SMXL clades has also been suggested (Khosla et al., 2020a). We found evidence for SMXL5-SMXL7 interactions in yeast two-hybrid assays, in split-luciferase complementation assays in *N. benthamiana*, and in the co-immunoprecipitation of FLAG-SMXL5 and GFP-SMXL7 expressed in Arabidopsis protoplasts (Figure 6D-F). Therefore, we could not exclude either hypothesis of how SMXL5 may inhibit AtD14-SMXL7 interactions, and it may be that both mechanisms occur.

An EAR motif is important for SMXL5 attenuation activity

We next explored the function of the EAR motif of SMXL5. The SMXL7 EAR motif has varying importance for different SL-regulated aspects of Arabidopsis development. Loss of the EAR motif has been proposed to reduce SMXL7 activity overall, or eliminate one of multiple mechanisms by which SMXL7 regulates different downstream processes (Liang et al., 2016). A *SMXL5* variant with a mutated EAR motif, $SMXL5^{mEAR}$, only partially

rescued the primary root growth defect of *smxl4,5* seedlings (Figure 7A; Supplemental Figure 3C). In further contrast to *SMXL5-YFP*, *SMXL5^{mEAR}-YFP* did not rescue the hypersensitive response to GR24^{5DS} in *smxl4,5* roots (Figure 7A). In this sense, *SMXL5^{mEAR}-YFP* had similar effects to *SMAX1-YFP* and *SMXL7-GFP* transgenes (Figure 2A). *SMXL5^{mEAR}-YFP* also partially rescued the increased anthocyanin phenotype of *smxl4,5* seedlings and the transcriptional response of *PRODUCTION OF ANTHOCYANIN PIGMENT2* (*PAP2*) to GR24^{5DS} (Supplemental Figure 9A-9C). However, *SMXL5^{mEAR}-YFP* did not rescue the reduced shoot branching phenotype of *smxl4,5* or its enhanced *BRC1* transcriptional response to GR24^{5DS} (Figure 7B-D). *SMXL5^{mEAR}* was also not as effective as *SMXL5* at inhibiting the expression of *pBRC1:LUC* in *N. benthamiana* leaves or its transcriptional upregulation by GR24^{5DS} (Supplemental Figure 9D). These data show that SMXL5^{mEAR} is hypomorphic.

Because EAR motifs are known to mediate interactions with TPL/TPR corepressor proteins (Causier et al., 2011; Leydon et al., 2021; Plant et al., 2021), the reduced ability of SMXL5^{mEAR} to rescue *smxl4,5* could result from loss of its transcriptional corepression activity on downstream target genes. However, *SMXL5^{mEAR}* also failed to restore normal responses to GR24^{5DS} in *smxl4,5* (Figure 7A and 7D; Supplemental Figure 9C and 9D), suggesting that the EAR motif may be important for attenuating SL responses. Therefore, we tested whether *SMXL5^{mEAR}* reduces SL-induced degradation of AtD14 and SMXL7 as effectively as *SMXL5*. In contrast to *SMXL5*, *SMXL5^{mEAR}* coexpression did not significantly slow the decline of either an AtD14 or SMXL7 ratiometric reporter after GR24^{5DS} treatment in *N. benthamiana* leaves (Figure 7E and 7F). Next, we investigated whether SMXL5^{mEAR} is able to interfere with AtD14-SMXL7 interactions. In pull-down assays, we found that *rac*-GR24-induced interactions between GST-AtD14 and MBP-SMXL7-GFP were less inhibited by the presence of GST-SMXL5^{mEAR} than by GST-SMXL5 (Figure 7G). Furthermore, coexpression of *SMXL5^{mEAR}* was less effective than *SMXL5* at inhibiting GR24^{5DS}-induced interactions between cLUC-AtD14 and SMXL7-nLUC in split-luciferase complementation assays (Figure 7H). As these assays use constitutive promoters (or none at all in the pull-downs), these observations suggest that

SMXL5^{mEAR} is less able to attenuate SL signaling due to a protein-protein interaction defect rather than a transcriptional regulation defect.

To investigate why SMXL5^{mEAR} has reduced SL attenuation activity, we tested protein-protein interactions between SMXL5^{mEAR}, AtD14, and SMXL7. In split-luciferase complementation assays, cLUC-AtD14 appeared to interact equally well with SMXL5^{mEAR}-nLUC or SMXL5-nLUC, both before and after GR24^{5DS} treatment (Figure 7I). Supporting this observation, GST-SMXL5 and GST-SMXL5^{mEAR} were similarly able to pull down His-GB-AtD14 in the presence of *rac*-GR24 (Supplemental Figure S9E). In contrast, SMXL7-nLUC showed less interaction with cLUC-SMXL5^{mEAR} than cLUC-SMXL5 (Figure 7J). Furthermore, in yeast two-hybrid assays SMXL5^{mEAR} did not interact with SMXL7, and a SMXL7^{mEAR} mutant did not interact with SMXL5 (Figure 7K). Finally, pull-down assays showed that GST-SMXL5^{mEAR} interacts with MBP-SMXL7-GFP less well than GST-SMXL5 does (Figure 7L). Collectively, these results indicate that the EAR motif strengthens SMXL5 interactions with SMXL7. This interaction appears to be important for SMXL5 to reduce SL-induced degradation of SMXL7 by AtD14-SCF^{MAX2}.

DISCUSSION

SL signaling activity is modulated by several mechanisms that may maintain SL homeostasis and modulate SL responses. Expression of SL biosynthesis genes and *SMXL6/7/8* is feedback-regulated in response to SL or nutrient abundance (Waters et al., 2017; Wang et al., 2020b). Sucrose inhibits SL-induced degradation of D53 and D14 in rice, whereas nitrate may enhance proteasomal degradation of D53 (Sun et al., 2021; Patil et al., 2022). Citrate can also act as an allosteric regulator of MAX2/D3 by affecting the positioning of the C-terminal helix (Tal et al., 2022). Here we have shown that SMXL5 and, putatively, SMXL4 provide another way to tune SL responses by inhibiting AtD14-SMXL7 interactions. Therefore, regulation of *SMXL4/5* expression or protein abundance may in turn be expected to tune SL responsiveness. Notably, *SMXL3/4/5* are expressed in phloem-related tissues, and there is potential overlap in *SMXL3/4/5* and *SMXL6/7/8* expression in the vasculature of mature roots and aerial tissues (Wallner et al., 2017; Soundappan et al., 2015). Also, the zinc-finger protein JULGI binds to the 5' UTR of

SMXL4 and *SMXL5* transcripts, inhibiting their translation (Cho et al., 2018). This raises the possibility that SL signaling is dampened in phloem or enhanced when *JULGI* is expressed. Tissue-specific modulation of SL signaling will be an exciting topic for future exploration.

Two features are likely to be important for SMXL5 to stabilize SMXL7 and AtD14 in the presence of SL. First, SMXL5 itself is resistant to SCF^{MAX2}-mediated degradation (Wallner et al., 2017), putatively because it lacks an RGKT motif. Consistent with this idea, a stabilized $SMAX1^{\Delta RGKT}$ mutant (Khosla et al., 2020a) had a similar ability to block AtD14-SMXL7 interactions as SMXL5 in split-luciferase assays (Supplemental Figure 10). However, for reasons we do not yet understand, $SMXL7^{\Delta RGKT}$ did not have the same effect. Second, the EAR motif is needed for full SMXL5 function. *SMXL5*^{mEAR} had a reduced ability to rescue the *smxl4,5* mutant, inhibit SL signaling, and block AtD14-SMXL7 interactions (Figure 7). $SMXL5^{mEAR}$ interactions with SMXL7, but not AtD14, were impaired, suggesting that SMXL5 protects SMXL7 from degradation primarily through SMXL5-SMXL7 association, rather than D14 sequestration (Figure 5). Also supporting this idea, SMXL5-D14 interactions are weak compared to SMXL7-D14 (Wang et al., 2020a; Figure 6A). At this time, however, we cannot exclude the contribution of D14-SMXL5 interactions to attenuation of SL signaling (Figure 5). Identifying a mutation that disrupts SMXL5 interactions with D14, but not SMXL7, would be useful to resolve this issue.

How might SMXL5-SMXL7 interactions be protective? One possibility is that SMXL protein monomers are more unstable or associate more readily with AtD14-SCF^{MAX2} than SMXL multimers (putatively, hexamers). For example, a AtD14 interaction domain might be inaccessible in SMXL-SMXL complexes. Notably, the C-terminal D2b domain of SMAX1, which is necessary and sufficient for SMAX1-SMAX1 interactions, is critical for the stability of SMAX1 ratiometric reporters that contain the RGKT degron motif (Khosla et al., 2020a). To speculate further, EAR motif-driven associations between SMXL and TPL/TPR proteins may reduce the dissociation of SMXL-SMXL complexes. Size-exclusion chromatography of recombinant GFP-D53 fusion proteins has shown a marked

increase in hexameric complexes relative to GFP-D53 monomers when the EAR motif-binding TPL domain (TPD) from TPR2 was included (Ma et al., 2017). The TPD also enables tetramerization of TPL/TPR proteins (Ke et al., 2015). A single TPL/TPR tetramer might therefore be able to interact with EAR motifs from multiple SMXL proteins at once, perhaps strengthening their association. Another recently raised, intriguing hypothesis is that chains of interactions between SMXL and TPR complexes might drive the formation of molecular condensates that alter SMXL activity (Temmerman et al., 2022). It is not yet clear, however, whether the EAR motif-dependent, SMXL5-SMXL7 two-hybrid interactions observed in yeast (Figure 7K) happen directly via the EAR motifs or involve association with a third party protein such as Tup1, a relative of TPL/TPR in *S. cerevisiae* (Causier et al., 2011; Leydon et al., 2021; Plant et al., 2021). Notably, a weakened interaction between SMXL5^{mEAR} and SMXL7 was observed in the *in vitro* pull-down assay (Figure 7L), which lacked TPL/TPR proteins or their homologs. This suggests a direct role for the EAR motif in enhancing SMXL5-SMXL7 interactions. In future work, it will be interesting to determine whether the EAR motif is important for protein-protein interactions between other clades of SMXL proteins.

The observation that SMAX1$^{\Delta RGKT}$ interferes with AtD14-SMXL7 interactions (Supplemental Figure 10) suggests that an attenuative function could evolve easily through similar mutations that confer resistance to SCF^{MAX2} and/or proteasomal degradation. At this time, it is unknown how common stabilized SMXL proteins are among land plants, but some speculation can be made based upon the presence or absence of the RGKT motif. All SMXL proteins in non-seed land plants (e.g. bryophytes, monilophytes) have the RGKT or a closely related, but functionally uncharacterized, RGRT (Arg-Gly-Arg-Thr) motif (Walker et al., 2019; Guillory et al., 2023). The SMXL4 and SMAX1 forms of SMXL proteins that emerged in the seed plant (spermatophyte) lineage retained this motif. The RGKT motif continued to be conserved in gymnosperm SMXL4 and SMAX1 proteins, as well as in the SMAX1 clade and its derivative SMXL78 clade in angiosperms. However, the RGKT motif was lost in the angiosperm aSMXL4 and SMXL39 clades, likely before their divergence (Walker et al., 2019). Thus, stabilized

SMXL proteins and their attendant function in SL signaling attenuation might be a unique feature of angiosperms.

It is likely that SCF^{MAX2}-dependent SL signaling was an innovation of seed plants that preceded the evolution of stabilized SMXL proteins in angiosperms, as the canonical receptor for SLs, D14, is found in both gymnosperms and angiosperms (Walker et al., 2019). However, outside of the seed plants, where D14 is absent, it is not clear that SL-induced degradation of SMXL proteins via SCF^{MAX2} occurs. It is certainly possible that some KAI2 homologs in non-seed plant lineages function as SL receptors, as has been observed among root parasitic angiosperms in the Orobanchaceae (Nelson, 2021). For example, in the moss *Physcomitrium patens*, the "GJM" clade of PpKAI2-L proteins are putative SL receptors (Lopez-Obando et al., 2021). However, the SMXL proteins in *P. patens* are not targeted for degradation by SL and do not repress SL responses. Instead, KL signaling triggers SMXL degradation via SCF^{MAX2} (Guillory et al., 2023). Similarly, the KAI2-SCF^{MAX2}-SMXL signaling mechanism is active in the liverwort *Marchantia polymorpha*, but SL perception and biosynthesis are absent (Mizuno et al., 2021; Walker et al., 2019). A related species, *Marchantia paleacea*, synthesizes a SL-like molecule, bryosymbiol, but this is used in communication with fungal symbionts rather than as a hormone (Kodama et al., 2022). Therefore, the emergence of stabilized SMXL proteins may have most closely coincided with the evolution of the SMXL78 clade of D14-SCF^{MAX2} target proteins in angiosperms.

We must be clear that attenuation of SL signaling is not the only function of degradation-resistant SMXL3/4/5 proteins, and therefore it may not have driven the evolutionary selection for RGKT mutants. Rather, SMXL3/4/5 proteins likely regulate a distinct set of transcriptional targets from SMAX1/SMXL2 and SMXL6/7/8 (Wallner et al., 2020), and perhaps benefit functionally from escaping regulation by SCF^{MAX2}. SMXL5 was recently shown to work with the PHD-finger protein OBERON3 to establish a phloem-specific developmental program through chromatin remodeling and expression of phloem regulatory proteins (Wallner et al., 2023). Furthermore, *SMXL5* misexpression could not

rescue *smax1 smxl2* or *smxl6,7,8* mutants, implying that SMXL5 controls the expression of different genes (Figure 1).

Why then could *SMAX1* and *SMXL7* rescue *smxl4,5* at least partially (Figure 2)? Additional *SMXL7* expression in *smxl4,5* may have helped correct a deficiency of *SMXL7* protein. Alternatively, perhaps SMAX1 and SMXL7 formed complexes with the remaining SMXL3 protein that strengthened its transcriptional regulation activity. Or, it might be that SMAX1 and SMXL7 can regulate a critical set of SMXL4/5 genomic targets, but not vice versa. Interestingly, two SMXL proteins from *P. patens* are also able to rescue the short root phenotype of *smxl4,5*, but not the hypocotyl elongation or shoot branching phenotypes of *smax1* and *smxl6,7,8*, respectively (Guillory et al., 2023). In this respect, the PpSMXL proteins show a partial complementation ability that is similar to misexpressed Arabidopsis SMAX1 and SMXL7 proteins. We favor the proposal of Guillory et al. (2023) that "the molecular function of SMXL could be conserved, but not their interaction network."

The SMXL domain(s) that specifies downstream outputs for the members of each clade awaits discovery. The potential formation of heterogeneous complexes composed of proteins from different SMXL clades also raises the interesting question of how specific gene regulatory networks could be controlled.

METHODS

Plant materials and growth conditions

The *Arabidopsis thaliana* mutants *smxl3-1*, *smxl4-1*, *smxl5-1*, *smxl4*,*5*, *smxl6*,*7*,*8*, *max2-1*, *Atd14-1* and transgenic lines *pSMXL5*:*SMXL5-YFP smxl4*,*5*; *pSMXL5*:*SMAX1-YFP smxl4*,*5*; and *pSMAX1:SMAX1-GFP smax1 smxl2* have been described previously (Waters et al., 2012; Stanga et al., 2013; Chevalier et al., 2014; Soundappan et al., 2015; Wallner et al., 2017; Khosla et al., 2020a). Arabidopsis seeds were surface-sterilized, stratified at 4 °C for 3 days, and germinated on 0.5× Murashige and Skoog (MS) medium containing 0.7% (w/v) agar. Plants were grown under white light (MaxLite LED T8 4000K, ~110 µmol m^{-2} s^{-1}) with LD photoperiod (16 h light/8 h dark) at 21°C. Soil was supplemented with Gnatrol WDG and Marathon (imidacloprid).

Plasmid construction and generation of transgenic plants

To construct *pSMXL5*:*SMXL7-GFP*, a 2768-bp fragment upstream from *SMXL5* (*AT5G57130*) start codon, a full-length *SMXL7* (*AT2G29970*) coding sequence (CDS) without stop codon, and a 720-bp *GFP* gene were amplified from Col-0 genomic DNA, Arabidopsis cDNA, and pGWB405 binary vector, respectively, using Primestar GXL high-fidelity DNA polymerase (Takara Bio) and primer pairs of pSMXL5-F and pSMXL5-7-R, SMXL7-F and SMXL7-G-R, and GFP-F and GFP-R, respectively. The construction of *pSMXL7*:*SMXL7-GFP* was the same as *pSMXL5*:*SMXL7-GFP* but used different primer pair pSMXL7-F and pSMXL7-7-R to amplify a 2664-bp fragment upstream from *SMXL7* start codon as the promoter. To construct *pSMAX1*:*SMXL5-YFP*, a 2747-bp fragment upstream from SMAX1 start codon and the sequence of *SMXL5-YFP* were amplified from the genomic DNA of Col-0 and *pSMXL5*:*SMXL5-YFP smxl4*,*5*, respectively, using Primestar GXL high-fidelity DNA polymerase (Takara Bio) and primer pairs of pSMAX1-F and pSMAX1-5-R, SMXL5-F and GFP-R, respectively. To construct *pSMXL7*:*SMXL5-YFP*, a 2664-bp fragment upstream from SMXL7 start codon and the sequence of *SMXL5-YFP* were amplified from the genomic DNA of Col-0 and *pSMXL5*:*SMXL5-YFP smxl4*,*5*, respectively, using Primestar GXL high-fidelity DNA polymerase (Takara Bio) and primer pairs of pSMXL7-F and pSMXL7-5-R, SMXL5-F and GFP-R, respectively. PCR products that used pSMXL5-F/SMXL5^{mEAR}-R and SMXL5^{mEAR}-F/GFP-R as primer

pairs and the genomic DNA of *pSMXL5*:*SMXL5 smxl4*,*5* as template were amplified to clone *pSMXL5*:*SMXL5*^{mEAR}-*YFP*. Corresponding fragments with overlapping sequences were assembled with each other and BamHI-SacI-digested pCAMBIA2300 using NEBuilder HiFi DNA Assembly Master Mix (New England Biolabs). The CDS of *SMXL5* was amplified by PCR with primer pairs of SMXL5-3C-F and SMXL5-3C-R and subsequently assembled with BamHI-EcoRI-digested pENTR3C using NEBuilder HiFi DNA Assembly Master Mix. Sequence-verified *SMXL5* was then cloned into pGWB541 binary vector using LR Clonase II Enzyme Mix (ThermoFisher) to generate *35S*:*SMXL5*-*YFP*. To construct *35S*:*D14*-*CFP*, *AtD14 (AT3G03990)* was cloned into pEarleyGate102 by a Gateway LR reaction. *Agrobacterium tumefaciens* (GV3101 pMP90)–mediated transformation of *Arabidopsis* was performed using the floral dip method as described previously (Clough and Bent, 1998). All characterized transgenic lines were homozygous in the T3 or higher generation and carried a single transgene insertion. Other new genotypes were assembled by crossing relevant existing genotypes, and were identified using PCR genotyping. All lines are in the Col-0 ecotype. Primers are listed in Supplemental Table 1.

Chemical compounds

KAR_2 and *rac*-GR24 were synthesized as previously reported (Goddard-Borger et al., 2007). $GR24^{5DS}$ enantiomer was purified from *rac*-GR24 by chiral-phase HPLC as described(Scaffidi et al., 2014). 10 mM stocks were prepared in acetone and stored at -20°C, and freshly diluted in aqueous solutions before use.

Branching assay

The position of plants within flats was randomized to account for environmental variation. The number of primary rosette branches, not including the primary shoot, at least 1 cm in length was measured for each plant at global proliferative arrest (~7 weeks after germination).

Root length assay

Seedlings were grown upright on the 0.5× MS agar containing 5 μM *rac*-GR24 or 0.1% (v/v) acetone and captured at 9 days after stratification. Primary root length was quantified using ImageJ (NIH).

Leaf morphology assay

The 7th leaf of each plant was harvested at ~4 weeks post stratification. The maximum length and width of the leaf blade were measured,

Anthocyanin content assay

5-day-old Arabidopsis seedlings were harvested, weighed and ground into powder in a bead mill. Anthocyanin was separated by incubating samples overnight in 300 μL methanol acidified with 1% HCl and then adding 200 μL distilled water and 500 μL chloroform. The anthocyanin content was indicated as ($A_{530} - A_{657}$) of the aqueous phase per gram of fresh weight.

RT-qPCR analysis

Total RNA was prepared and DNAse-treated with the Spectrum Plant Total RNA Kit and On-Column DNase I Digestion Set (Sigma-Aldrich) from 7-day-old seedlings grown in LD photoperiod. First-strand cDNA was synthesized from 2 μg of total RNA with the Verso cDNA Synthesis Kit (ThermoFisher). Quantitative PCR was performed in a CFX384 Real-Time PCR Detection System (Bio-Rad) using Luna Universal qPCR Master Mix (New England Biolabs) with the following program: 5 min at 95°C and 45 cycles of 20 s at 95°C, 20 s at 60°C, and 20 s at 72°C, followed by melt curve analysis to analyze product specificity. The relative expression was calculated as previously described (Wang et al., 2020b; Li et al., 2022).

Transient Expression in *Nicotiana benthamiana*

N. benthamiana plants (3-week-old) were used to express the various construct combinations by Agrobacterium (GV3101 pMP90)–mediated transient transformation of lower epidermal leaf cells as described previously (Khosla et al., 2020a).

Transcriptional activity assay in *N. benthamiana*

To construct the recombinant plasmids used in transcriptional activity assays, a 3 kb fragment upstream from *BRC1* start codon and the CDS of *redLUC* were amplified, and cloned into digested pGWB402 as a reporter. *SMXL5* or *SMXL5*^{mEAR} was cloned into pGWB541 as an effector. To detect regulation of effector on the *BRC1* promoter activity through SMXL7, we co-expressed *pBRC1*:*LUC* reporter, *35S*:*SMXL5-YFP* or *35S*:*SMXL5*^{mEAR}*-YFP* effector and *35S*:*SMXL7-FLAG* in *N. benthamiana* leaves. The *Agrobacterium tumefaciens* strain containing *35S*:*mCherry* was used as a control. After 3 d, leaf discs were excised and immersed into 150 µL of 2 mM luciferin solution with 10 µM GR24^{5DS} in a 96-well white plate (PE OptiPlate 96, PerkinElmer) and kept in the dark for 5 min before measurement. Luminescence was measured using the emission filter 580 nm (80 nm bandwidth) in a CLARIOstar plate reader (BMG Labtech) and normalized to fluorescence of mCherry transformation control (ex. 570-15 nm, em. 620-20 nm).

Degradation assays in *N. benthamiana*

To generate ratiometric reporter constructs for degradation assays in *N. benthamiana*, *D14, SMXL7*, and *SMXL7*^{mEAR} entry clones were transferred into the pRATIO1212 destination vector by Gateway LR reaction (Khosla et al., 2020b; Soundappan et al., 2015). To examine the time-course of degradation, the wells of a black 96-well polystyrene plate (PE OptiPlate 96, PerkinElmer) were filled with 150 µl chemical treatments (10 µM GR24^{5DS} or 0.1% (v/v) acetone). Leaf discs were excised 3 d post-infiltration and transferred to the treatment plate (one leaf disc per well) with the abaxial side up. Relative fluorescence was measured in a CLARIOstar plate reader (BMG Labtech) in plate mode (slow kinetics) at the indicated time points with the following settings: spiral scan option; scan diameter (mm), 5; and number of flashes per well per cycle, 36. Optimal settings for fluorescence measurements of the mScarlet-I reporter (ex. 560-10 nm, em. 595-10 nm) and Venus reference (ex. 497-15 nm, em. 540-20 nm) proteins were described previously (Khosla et al., 2020b). Degradation was quantified as mScarlet-I/Venus fluorescence intensity ratios after subtracting background fluorescence signals measured in leaf discs transformed with RNA silencing suppressor P19.

Protein degradation assay in *Arabidopsis thaliana*

The 7-day-old *35S*:*D14-CFP and pSMXL7*:*SMXL7-GFP* transgenic plants (Col-0, *smxl4,5* or *max2 smxl4,5* background) were treated with 5 μM $GR24^{5DS}$ or 0.1% (v/v) acetone for the indicated times in 0.5× MS liquid medium at 21 °C. Equal weights of plant materials were collected for protein extraction using lysis buffer (50 mM Tris-HCl at pH 8.0, 150 mM NaCl, 10% glycerol, 1% Nonidet P-40, 2 mM EDTA) containing 1× complete protease-inhibitor cocktail (Roche). Protein levels of D14-CFP and SMXL7-GFP were detected by immunoblotting with rabbit anti-GFP polyclonal antibody (Abcam) and mouse anti-GFP monoclonal antibody (Roche), respectively. Blots were probed with Radiance Plus Femtogram HRP Substrate (Azure biosystems) and visualized on a Azure 300 imaging system (Azure biosystems). Experiments were repeated independently three times. Relative abundance of SMXL7-GFP and D14-CFP was quantified using ImageJ software (NIH).

Yeast two-hybrid and three-hybrid assays

The coding sequences of *AtD14*, *SMXL7* and *SMXL5* were cloned into yeast expression vectors pGBKT7 and pBridge (Takara Bio). *SMXL5* was further cloned into the pBridge-AtD14 to co-express *SMXL5* under the control of the promoter of *Met25*. *ASK1 (AT1G10940)* fused with the N-terminus of *MAX2* (*AT2G42620*) was cloned into pGADT7 to create a pGADT7-ASK1-MAX2 construct. The sequences of SMXL5 EAR motif 'LDLNI' and SMXL7 EAR motif 'LDLNL' were modified to 'ADANA'. *SMXL5*, $SMXL5^{mEAR}$, *SMXL7* and $SMXL7^{mEAR}$ were then cloned into pGADT7 to obtain pGADT7-SMXL5, pGADT7-$SMXL5^{mEAR}$, pGADT7-SMXL7 and pGADT7-$SMXL7^{mEAR}$.

Y2H was performed following the instruction of Yeastmaker Yeast Transformation System 2 (Clontech). Bait and prey constructs were co-transformed into the yeast strain AH109 or Y2HGold by the lithium acetate-mediated method (Gietz and Woods, 2002). The transformed yeast cells were plated on selective growth medium SD/-Leu-Trp for 3 d at 30°C. Interactions in yeast were tested on selective growth medium SD/-Leu-Trp-His, SD/-Leu-Trp-His in the presence of 3-AT or AbA and SD/-Leu-Trp-His-Ade.

For Y3H assay, pBridge-AtD14-SMXL5 was co-transformed with pGADT7-SMXL7 or pGADT7-ASK1-MAX2 into AH109 cells by the lithium acetate-mediated method. The transformed yeast cells were plated on selective growth medium SD/-Leu-Trp for 3 d at 30°C. Serial 10-fold dilutions (from OD_{600} 2.5) of positive transformants were spotted onto selective growth mediums SD/-Leu-Trp-His-Ade, SD/-Leu-Trp-His-Ade-Met and SD/-Leu-Trp-His-Ade-Met re-supplemented with 640 μM Met in the presence of 5 μM *rac*-GR24 or mock control. Yeast cells were then grown at 30°C for 3 d to observe the effect of SMXL5 on AtD14 interactions with SMXL7 and ASK1-MAX2.

Split-luciferase complementation assay

To construct plasmids used in the assay, *AtD14*, *Atd14*^{S97A}, *SMXL5* and *SMXL5*^{mEAR} were cloned into pCAMBIA1300-cLUC, and *SMXL7* and *SMXL5* were cloned into pCAMBIA1300-nLUC using NEBuilder (Chen et al., 2008). The various combinations of nLUC and cLUC fusion plasmids were then transformed into *N. benthamiana* leaves. The Agrobacterium strain containing *35S*:*mCherry* was used as a transformation control. After 3 d, leaf discs were excised and immersed into 150 μL of 2 mM luciferin solution with 10 μM GR24^{5DS} in a 96-well white plate (PE OptiPlate 96) and kept in the dark for 5 min before measurement. Luminescence was measured using the emission filter 580 nm (80 nm bandwidth) and normalized to fluorescence of mCherry.

Pull-down assay

The coding sequences of *AtD14* and a *AtD14*^{S97A} variant were cloned into pET-28a (+) and pGEX-6P-1, resulting in *His-AtD14*, *His-AtD14* ^{S97A} and *GST-AtD14* fusions. The CDS of *SMXL5* and *SMXL5*^{mEAR} was cloned into pGEX-6P-1 to generate *GST-SMXL5* and *GST-SMXL5*^{mEAR} fusions. The CDS of *SMXL7* was cloned into pETL8 which was remold with GFP in C-terminal of multiple cut-sites (MCS) to generate a *MBP-SMXL7-GFP* fusion. All constructs were transformed into *Escherichia coli* BL21(DE3). Fusion proteins were induced by Isopropyl β-D-1-thiogalactopyranoside (IPTG; 0.5 mM) at 16°C for 16 h, and purified using Glutathione beads 4FF, MBP beads or Ni Sepharose™ 6 Fast Flow (GE HealthCare) (Yao et al., 2018).

To investigate the interaction between AtD14 and SMXL5 or SMXL5^{mEAR}, purified GST-SMXL5 (40 μg) or GST-SMXL5^{mEAR} (40 μg) were co-incubated with His-AtD14 (10 μg) in 300 μL binding buffer (50 mM Tris-HCl, 100 mM NaCl, 10% [v/v] glycerol, 20 mM β-mercaptoethanol, 0.1% [v/v] Tween20, pH 6.8) in the presence or absence of 20 μM *rac*-GR24 at 20°C for 1 h. 50 μL GST beads were added to mixtures, followed by incubation at 4°C with gentle rotation for 30 min. After washing 8-10 times, the protein complexes on beads were released. The samples were then analyzed by Western blot using anti-His antibody (Abmart).

To investigate the interaction between SMXL7 and SMXL5 or SMXL5^{mEAR}, purified GST-SMXL5 (40 μg) or GST-SMXL5^{mEAR} (40 μg) protein and were co-incubated with MBP-SMXL7-GFP (10 μg) in 300 μL binding buffer at 20°C for 1 h. 50 μL GST beads were added to the reaction mixtures, followed by incubation at 4°C with gentle rotation for 30 min. After washing 8-10 times, the protein complexes on beads were released. The samples were then analyzed by Western blot using anti-GFP antibody (Roche).

For competitive GST pull-down assay, GST-SMXL5 or GST-SMXL5^{mEAR} were digested at 4 °C for 16 h to obtain SMXL5 or SMXL5^{mEAR}. SMXL5 (20 μg) or SMXL5^{mEAR} (20 μg) was added to the mixture that contained GST-AtD14 (40 μg) and MBP-SMXL7-GFP (10 μg), and incubated in 300 μL binding buffer in the presence or absence of 20 μM *rac*-GR24 at 20°C for 1 h. 50 μL GST beads were added to the mixtures, followed by incubation at 4°C with gentle rotation for 30 min. After washing 8-10 times, the protein complexes on beads were released. The samples were then analyzed by Western blot using anti-GFP antibody (Roche).

Co-immunoprecipitation assay

To generate *35S*:*3×HA-SMXL7*, *35S*:*GFP-SMXL7* and *35S*:*3×Flag-AtD14* plasmids, *SMXL7* and *AtD14* cloned into the pBeacon-3×HA, pBeacon-eGFP and pBeacon-3×Flag transient vector by Gateway LR reaction (Wang et al., 2015). The coding sequence of *SMXL5* was amplified by PCR with primer pairs of pDSMXL5-F and pDSMXL5-R, and subsequently cloned into pBeacon-3×Flag transient vector by Gateway LR reaction to

construct *35S*:*3×Flag-SMXL5* plasmid. The Arabidopsis protoplasts of Col-0 or *35S*:*SMXL5-YFP* transgenic plants for *in vivo* Co-IP assays were prepared using mesophyll cells of 4-week-old rosette leaves grown under 10 h light/14 h dark as described (Yoo et al., 2007), followed by the transfection with a series of combinations of constructs. After the incubation in W5 solution (154 mM NaCl,125 mM $CaCl_2$, 5 mM KCl, 2 mM MES [pH 5.7]) in darkness for 11 h, protoplasts were treated with DMSO or 100 μM $GR24^{4DO}$ for 1 h. Then protoplasts were collected and lysed in 1ml of protein lysis buffer containing 50 mM Tris-HCl (pH 7.5), 150 mM NaCl, 10% (v/v) glycerol, 0.1% (v/v) Nonidet P-40, and 1×EDTA-free protease inhibitor cocktail (Roche). After 15 min centrifugation at 17000 *g*, 4°C, 70 μl lysate supernatants were used as input, and the rest incubated with 15 μL anti-HA-tag mAb-Magnetic Agarose (MBL) at 4°C for 3 h in the presence or absence of $GR24^{4DO}$ treatment. The HA-agarose were then washed 4 times with washing buffer (50 mM Tris-HCl [pH 7.5], 150 mM NaCl, 10% [v/v] glycerol, 0.01% [v/v] Nonidet P-40) and protein were eluted into SDS loading buffer (100 mM Tris-HCl [pH 6.8], 0.4% [w/v] SDS, 10% [v/v] glycerol, 10% [v/v] β-mercaptoethano, 0.2% [w/v] bromophenol blue). Mouse anti-GFP monoclonal antibody (Roche) at a 1:3000 dilution, Mouse anti-HA monoclonal antibody (CWBIO) at a 1:3000 dilution and Mouse anti-DDDDK monoclonal antibody (MBL) at a 1:4000 dilution were used for Western blot to detect the GFP-SMXL7, HA-SMXL7, Flag-SMXL5 and Flag-AtD14, respectively.

Statistical analysis

Data were analyzed by using JMP Pro v16 and Excel. For multiple comparisons of means, one-way ANOVA was performed followed by Student-Newman-Keuls test ($p < 0.05$ cutoff for significance). Two-sided Student's t-test was conducted for comparisons of means between two groups. Graphs were produced using Prism v9 (GraphPad Software). Box plots show the median, 25th percentile, and 75th percentile. Tukey whiskers on box plots extend 1.5 times the interquartile range beyond the 25th/75th percentile up to the minimum/maximum value in the data set. Outlier data beyond Tukey whiskers are shown as individual points. For sample sizes with n = 3, individual data points and the mean value are shown.

ACKNOWLEDGMENTS

Funding for this project was provided by the National Science Foundation, Division of Integrative Organismal Systems (grants 1737153, 1740560, 1856741) to DCN; the Hainan Yazhou Bay Seed Lab (grant B23C19701) to QL; the National Key Research and Development Program of China (grant 2021YFA1300400), the National Natural Science Foundation of China (grant 32070321), and Shenzhen Science and Technology Innovation Commission (grant 2021Szvup037) to RY; the National Natural Science Foundation of China (grant 32170320) and Hebei Natural Science Foundation (grant C2022503003) to LW; and Deutsche Forschungsgemeinschaft (grant GR 2104/9-1) to TG. KAR_2, *rac*-GR24, and $GR24^{5DS}$ were kindly provided by Dr. Adrian Scaffidi and Dr. Gavin Flematti (University of Western Australia).

CONTRIBUTIONS

Experiments were designed, carried out, and analyzed by QL, HY, WC, LF, SC, E-SW, MG and HY. Figure preparation by QL. Manuscript preparation by QL and DCN with contributions and final approval from all authors. Project design by QL, LW, RY, TG, and DCN. Funding to support the project was secured by QL, RY, TW, TG, and DCN.

COMPETING INTERESTS

The authors declare no competing interests.

FIGURE LEGENDS

Figure 1. SMXL5 cannot functionally replace SMXL proteins of other clades.

(A) Hypocotyl lengths of 5-day-old seedlings of Col-0, *smax1 smxl2*, two independent *pSMAX1*:*SMXL5-YFP smax1 smxl2* transgenic lines and two independent *pSMAX1*:*SMAX1-GFP smax1 smxl2* transgenic lines grown under continuous red light for 4 days on 0.5× MS medium containing 1 μM KAR_2, 1 μM *rac*-GR24, or mock control. Bar = 5 mm.

(B) Blade length (white), not including the petiole, width (blue) and length:width ratio (orange) of the 7th leaf of 35-day-old Col-0, *smxl6*,*7*,*8*, two independent *pSMXL7*:*SMXL5-YFP smxl6*,*7*,*8* transgenic plants and two independent *pSMXL7*:*SMXL7-GFP smxl6*,*7*,*8* transgenic plants.

(C) Number of rosette and cauline branches of plants in **(B)**.

(D) Adult shoot morphology of plants in **(C)**. Bar = 10 cm.

Box-and-whisker plots in **(A)**, **(B)**, and **(C)** with the same letter are not significantly different from one another (Student-Newman-Keuls test, $p < 0.05$). Lowercase, uppercase and single quotation marks differentiate statistical tests of measurements.

Figure 2. Loss of *SMXL4* and *SMXL5* enhances strigolactone responses.

(A) Primary root lengths of 9-day-old wild-type (Col-0); *smxl4*,*5*; two independent transgenic lines of *pSMXL5*:*SMXL5-YFP smxl4*,*5*; *pSMXL5*:*SMAX1-YFP smxl4*,*5*; and *pSMXL5*:*SMXL7-GFP smxl4*,*5* plants grown on 0.5× MS agar containing mock (solvent control), 2 μM $GR24^{5DS}$, 5 μM $GR24^{5DS}$, 2 μM KAR_2 or 5 μM KAR_2. n = 14-20.

(B) Adult shoot morphology of wild-type (Col-0); *smxl3*; *smxl4*; *smxl5*; *smxl3*,*4*; *smxl3*,*5*; *smxl4*,*5*; two independent transgenic lines of *pSMXL5*:*SMXL5-YFP smxl4*,*5*; *pSMXL5*:*SMAX1-YFP smxl4*,*5*; *pSMXL5*:*SMXL7-GFP smxl4*,*5*; *Atd14*; *Atd14 smxl4*,*5*; *max2*; and *max2 smxl4*,*5* at the proliferative stage (~7-week-old) grown under white light (~110 μmol m^{-2} s^{-1}) with 16-h-light/8-h-dark photoperiod at 21°C. Bar = 10 cm.

(C) Primary rosette branch number of indicated genotypes shown in **(B)**. n = 10-15.

(D) RT-qPCR analysis of *BRC1* gene expression in nonelongated axillary buds of Col-0, *smxl4*,*5*, *smxl6*,*7*,*8*, *max2 smxl4*,*5*, and *max2 smxl6*,*7*,*8*. *BRC1* transcript level is relative to *CACS* internal reference gene transcripts.

(E) RT-qPCR analysis of *SMXL7* gene expression in nonelongated axillary buds of Col-0, *smxl4*,*5*, *smxl6*,*7*,*8*, *max2 smxl4*,*5*, and *max2 smxl6*,*7*,*8*. *SMXL7* transcript level is relative to *CACS* internal reference gene transcripts.

(F) RT-qPCR analysis of *BRC1* transcripts in 7-day-old seedlings of Col-0; *smxl4*,*5*; *pSMXL5*:*SMXL5 smxl4*,*5*; *Atd14 smxl4*,*5*; and *max2 smxl4*,*5* after 3 h treatment with 5 µM $GR24^{5DS}$ or mock control. *BRC1* transcript level is relative to *CACS* internal reference gene transcripts.

(G) The *pBRC1*:*LUC* reporter activity with the presence or absence of SMXL5 in wt tobacco and *Nbd14a*,*b*. SMXL7 was co-expressed. Leaf discs were treated with 10 µM $GR24^{5DS}$ for 3 h. Luminescence was normalized to mCherry internal control. n = 10 leaf discs.

Bars in **(D)**, **(E)** and **(F)** indicate the mean. n = 3 pooled tissue samples. Asterisks in **(D)**, **(E)** and **(F)** indicate significant differences between mock and treated samples within genotype using Student's t test (*$p < 0.05$ or **$p < 0.01$; ns indicates no significance).

Box-and-whisker plots in **(A)**, **(C)** and **(G)** with the same letter are not significantly different from one another (Student-Newman-Keuls test, $p < 0.05$).

Figure 3. SMXL4 and SMXL5 attenuate $GR24^{5DS}$-induced degradation of SMXL7 and AtD14.

(A) Relative abundance of SMXL7-GFP in Col-0, *smxl4*,*5* and *max2 smxl4*,*5* after 5 min treatment of 5 µM $GR24^{5DS}$ or mock control determined by Western blot densitometry of blot shown in Supplemental Figure **8A**.

(B) Time course assay of SMXL7 stability in *N. benthamiana* under 10 µM $GR24^{5DS}$ treatment. Relative fluorescence from the SMXL7-mScarlet-I reporter with the presence or absence of SMXL5 after co-expressing AtD14 or $Atd14^{S97A}$ in *Nbd14a*,*b* is shown. n = 18 leaf discs. Asterisks indicate significant differences to each group at 0 h using Student's t test (*$p < 0.05$ and **$p < 0.01$).

(C) Relative abundance of AtD14-CFP in Col-0, *smxl4*,*5* and *max2 smxl4*,*5* after 4 h treatment of 5 µM $GR24^{5DS}$ or mock control determined by Western blot densitometry of blot shown in as shown in Supplemental Figure **8C**.

(D) Time course assay of AtD14 and Atd14^{S97A} stability in *N. benthamiana* under 10 µM GR24^{5DS} treatment. Relative fluorescence from the AtD14-mScarlet-I reporter and Atd14^{S97A}-mScarlet-I reporter after co-expressing an empty vector (EV) or SMXL5 in *Nbd14a*,*b* is shown. n = 10 leaf discs. Asterisks indicate significant differences to each group at 0 h or between compared pairs using the Student's t test (*p < 0.05 and **p < 0.01; ns indicates no significance).

Relative abundance of SMXL7-GFP in **(A)** and AtD14-CFP in **(C)** determined by densitometry was normalized to respective loading controls, with the zero-time signal set as 1.00. n = 3 experimental replicates (three independently prepared genotype-treatment protein samples analyzed on separate immunoblots). Bars indicate the mean. Asterisks indicate significant differences to each mock or between compared pairs using Student's t test (*p < 0.05 and **p < 0.01).

Figure 4. SMXL5 inhibits AtD14-SMXL7 association.

(A) Yeast three-hybrid assay of AtD14-SMXL7 or AtD14-ASK1-MAX2 interaction in the absence or presence of SMXL5. AtD14 was fused to GAL4-BD. SMXL7 and ASK1-MAX2 were fused to GAL4-AD. *SMXL5* expression was driven by the *MET25* promoter. Serial 10-fold dilutions of yeast cultures starting from OD_{600} 2.5 were spotted onto selective growth medium (-L, -Leu; -T, -Trp; -H, -His; -A, -Ade; -M, -Met) that was supplemented with 5 µM *rac*-GR24 or mock control. Methionine was re-supplemented into -LTHAM medium as indicated to suppress the *MET25* promoter activity.

(B) Effect of SMXL5 on interaction of AtD14 and SMXL7 was detected in the split-luciferase complementation assay. *N. benthamiana* leaves were transiently co-transformed with *Agrobacterium tumefaciens* strains carrying cLUC, nLUC, or indicated fusions as well as a strain carrying an mCherry transgene as a transformation control. + and – indicate *35S*:*SMXL5-YFP* and *35S*:*GFP*, respectively. Luminescence was measured before and 1 hour after treatment with 10 µM GR24^{5DS}, and was normalized against mCherry fluorescence. n = 10-12 leaf discs. Box-and-whisker plots with the same letter are not significantly different from one another (Student-Newman-Keuls test, p < 0.05).

(C) Association of Flag-AtD14 with HA-SMXL7 revealed by Co-IP assay (IP) in protoplasts of wild-type (Col-0) or *35S*:*SMXL5*-*YFP* transgenic plants in the absence or presence of 100 μM $GR24^{4DO}$. The Flag-AtD14 and HA-SMXL7 fusion proteins were detected with anti-Flag monoclonal antibody and anti-HA monoclonal antibody, respectively. Relative abundances of Flag-AtD14 after immunoprecipitation were determined by densitometry with the signal from Col-0 protoplasts in the absence of $GR24^{4DO}$ set as 1.00.

Figure 5. Two hypotheses of how SMXL5 attenuates strigolactone signaling.

(A) A model of strigolactone signaling. After binding and/or hydrolysis of strigolactone, AtD14 associates with SCF^{MAX2} and target proteins such as SMXL7. The target(s) are polyubiquitinated and then destroyed by the 26S proteasome, relieving transcriptional repression by SMXL proteins. We propose that SMXL proteins form multimeric complexes (here shown as a hexamer) that can also dissociate into monomers. SMXL proteins can interact with TPL/TPR (yellow, "T") via a C-terminal EAR motif, which can promote the formation or stability of SMXL multimers (Ma et al., 2017). TPL/TPR proteins are known to impose transcriptional repression through interaction with histone deacetylases, the Mediator complex, and/or histone proteins (not depicted). SMXL proteins may bind DNA directly or indirectly through interaction with transcription factors (not depicted). *BRC1* is shown as an example of a downstream transcriptional target of SMXL7. *BRC1* inhibits axillary bud outgrowth (branching). It is not yet known whether SMXL proteins function as transcriptional corepressors with TPL/TPR in monomeric and/or multimeric states. It is also unknown whether AtD14-SCF^{MAX2} targets SMXL protein monomers, multimers, or both. As drawn, this cartoon proposes that SMXL monomers are targeted for degradation and SMXL multimers regulate gene expression.

(B) The D14 sequestration hypothesis proposes that SMXL5, which is resistant to MAX2-dependent degradation, forms non-productive interactions with AtD14-SCF^{MAX2} that competitively interfere with AtD14-SCF^{MAX2} targeting of SMXL7. This results in an increase in SMXL7 abundance and reduced SL responses.

(C) The SMXL complex stabilization hypothesis proposes that SMXL7 is somehow less susceptible to targeting by AtD14-SCF^{MAX2} when it forms heteromeric complexes with

SMXL5. For example, SMXL5 might promote multimer formation or reduce multimer dissociation, causing an equilibrium shift toward multimeric SMXL7 and increased SMXL7 abundance.

Figure 6. SMXL5 physically interacts with AtD14 and SMXL7.

(A) Yeast two-hybrid assays of SMXL5 interactions with AtD14 and Atd14^{S97A} using yeast strain Y2HGold. AtD14 and Atd14^{S97A} were fused to GAL4-BD. SMXL5 and SMXL7 were fused to GAL4-AD. 100 ng/mL Aureobasidin A (AbA) was added into -LTH medium for more stringent selection. Serial 10-fold dilutions of yeast cultures starting from OD_{600} 1.0 were spotted onto selective growth medium supplemented with 2 μM GR24^{5DS} or mock control.

(B) Split-luciferase complementation assay for SMXL5 interactions with AtD14 and Atd14^{S97A}. Luminescence was measured before and 1 hour after treatment with 10 μM GR24^{5DS}, and was normalized against mCherry fluorescence. n ≥ 12 leaf discs.

(C) The *in vitro* GST pull-down assay of GST-SMXL5 and His-GB1-AtD14 or His-GB1-Atd14^{S97A} in the presence or absence of *rac*-GR24. Recombinant proteins were resolved by SDS-PAGE and were visualized via Western blot with anti-His antibody. Panels of GST pull-down and input share the same molecular markers.

(D) Yeast two-hybrid assays for investigating heterodimerization or homodimerization of SMXL5 and SMXL7. 0.1 mM 3-Amino-1,2,4-triazole (3-AT) was added to -LTH medium to reduce background growth. Serial 10-fold dilutions of yeast cultures starting from OD_{600} 2.5 were spotted onto selective growth medium.

(E) Split-luciferase complementation assay for SMXL5 interaction with SMXL7. n = 10-15 leaf discs.

(F) Association of Flag-SMXL5 with GFP-SMXL7 revealed by Co-IP assay (IP) in protoplasts of wild-type (Col-0) in the absence or presence of 100 μM GR24^{4DO}. The Flag-SMXL5 fusion protein was detected with anti-Flag monoclonal antibody; the GFP-SMXL7 fusion protein and GFP were detected with anti-GFP monoclonal antibody.

Box-and-whisker plots in **(B)** and **(E)** with the same letter are not significantly different from one another (Student-Newman-Keuls test, $p < 0.05$).

Figure 7. Attenuation of SL signaling by SMXL5 requires the EAR motif.

(A) Root lengths of 9-day-old wild-type (Col-0); *smxl4*,*5*; two independent transgenic lines of *pSMXL5*:*SMXL5-YFP smxl4*,*5*; and two independent transgenic lines of *pSMXL5*:*SMXL5*^{mEAR}*-YFP smxl4*,*5* (SMXL5 variant with a mutated EAR motif, sequence LDLNI modified to ADANA) plants grown on the 0.5× MS agar containing mock, 2 μM GR24^{5DS} or 5 μM GR24^{5DS}. n = 16-20. Bar = 10 mm. Images and data of wild-type (Col-0); *smxl4*,*5*; and two independent transgenic lines of *pSMXL5*:*SMXL5-YFP smxl4*,*5* are duplicated in Supplemental Figure 4 and Figure **2A**, respectively, which were done together in the same experiment.

(B) Adult shoot morphology of wild-type (Col-0); *smxl4*,*5*; two independent transgenic lines of *pSMXL5*:*SMXL5-YFP smxl4*,*5*; and two independent transgenic lines of *pSMXL5*:*SMXL5*^{mEAR}*-YFP smxl4*,*5* at the proliferative stage (~7-week-old) grown under white light (~110 μmol m^{-2} s^{-1}) with 16-h-light/8-h-dark photoperiod at 21°C. Bar = 10 cm.

(C) Primary rosette branch number of indicated genotypes shown in **(B)**. n = 10-15.

(D) RT-qPCR analysis of *BRC1* gene expression in 7-day-old seedlings of wild-type (Col-0); *smxl4*,*5*; *pSMXL5*:*SMXL5-YFP smxl4*,*5* #1; and *pSMXL5*:*SMXL5*^{mEAR}*-YFP smxl4*,*5* #1 after 3 h treatment of 5 μM GR24^{5DS} or mock control. *BRC1* transcript level is relative to *CACS* internal reference gene transcripts. Bars indicate the mean. n = 3 pooled tissue samples. Asterisks indicate significant differences to each mock or between compared pairs using Student's t test (**p < 0.01; ns indicates no significance).

(E) Time course assay of AtD14 stability in *N. benthamiana* under 10 μM GR24^{5DS} treatment. Relative fluorescence from the AtD14-mScarlet-I reporter with SMXL5 or SMXL5^{mEAR} in wt tobacco is shown. n = 17 leaf discs.

(F) Time course assay of SMXL7 stability in *N. benthamiana* under 10 μM GR24^{5DS} treatment. Relative fluorescence from the SMXL7-mScarlet-I reporter with SMXL5 or SMXL5^{mEAR} after co-expressing AtD14 in *Nbd14a*,*b* is shown. n = 12 leaf discs.

(G) The *in vitro* competitive GST pull-down assay of GST-AtD14 and MBP-SMXL7-GFP in the presence or absence of *rac*-GR24, SMXL5 or SMXL5^{mEAR}. Relative abundance of MBP-SMXL7-GFP was determined by densitometry, with the signal from GST pull-down in the presence of GST-AtD14, MBP-SMXL7-GFP and *rac*-GR24 set as 1.00.

(H) Repression of AtD14-SMXL7 association by SMXL5 or SMXL5^{mEAR} was assessed by split-luciferase complementation assay. n = 12 leaf discs.

(I) Split-luciferase complementation assay for AtD14 interactions with SMXL5 and SMXL5^{mEAR}.

(J) SMXL7 interactions with SMXL5 and SMXL5^{mEAR} were assessed by split-luciferase complementation assay. n = 10-15 leaf discs. Asterisks indicate significant difference using the Student's t test (**p < 0.01).

(K) Yeast two-hybrid assays for SMXL5^{mEAR}-SMXL7 and SMXL5-SMXL7^{mEAR} interactions. 0.5 mM 3-AT was added into -LTH medium to reduce background growth. Serial 10-fold dilutions of yeast cultures starting from OD_{600} 2.5 were spotted onto selective growth medium.

(L) The *in vitro* GST pull-down assay of MBP-SMXL7-GFP and GST-SMXL5 or GST-SMXL5^{mEAR}. Relative abundance of MBP-SMXL7-GFP was determined by densitometry, with the signal from GST pull-down in the presence of GST-SMXL5 and MBP-SMXL7-GFP set as 1.00.

Images in **(B)** and data in **(C)** of wild-type (Col-0); *smxl4*,*5*; and two independent transgenic lines of *pSMXL5*:*SMXL5-YFP smxl4*,*5* are duplicated in Figure **2B** and **2C**, respectively, which were done together in the same experiment.

Box-and-whisker plots in **(A)**, **(C)**, **(H)** and **(I)** with the same letter are not significantly different from one another (Student-Newman-Keuls test, p < 0.05).

Asterisks in **(E)** and **(F)** indicate significant differences to EV control at each time point using the Student's t test (*p < 0.05 and **p < 0.01; ns indicates no significance).

In **(H)**, **(I)** and **(J)**, *N. benthamiana* leaves were transiently co-transformed with *Agrobacterium tumefaciens* strains carrying cLUC, nLUC, or indicated fusions as well as a strain carrying an mCherry transgene as a transformation control. Luminescence was measured without treatment or before and 1 hour after treatment with 10 μM GR24^{5DS}, and was normalized against mCherry fluorescence.

In **(G)** and **(L)**, recombinant proteins were resolved by SDS-PAGE and were visualized via Western blot with anti-GFP antibody. MBP-GFP was used as a control. Panels of GST pull-down and input share the same molecular markers.

SUPPLEMENTAL FIGURE LEGENDS

Supplemental Figure 1. Expression of *SMXL* transgenes in Arabidopsis transgenic lines.

(A) RT-qPCR analysis of *SMAX1* and *SMXL5-YFP* transcripts in 7-day-old seedlings of Col-0, *smax1 smxl2* and two independent *pSMAX1*:*SMXL5-YFP smax1 smxl2* transgenic lines.

(B) RT-qPCR analysis of *SMXL7* and *SMXL5-YFP* transcripts in 7-day-old seedlings of Col-0, *smxl6,7,8* and two independent *pSMXL7*:*SMXL5-YFP smxl6,7,8* transgenic lines.

(C) RT-qPCR analysis of *SMXL7* transcripts in 7-day-old seedlings of Col-0, *smxl6,7,8* and two independent *pSMXL7*:*SMXL7-YFP smxl6,7,8* transgenic lines.

In **(A)**, **(B)** and **(C)**, *SMAX1*, *SMXL7* and *SMXL5-YFP* transcript levels are relative to *CACS* internal reference gene transcripts. Bars indicate the mean. n = 3 pooled tissue samples.

Supplemental Figure 2. *SMXL7* complements *smxl4,5* but not *smxl3,4,5*.

(A) Growth of 4-week-old plants. *smxl3,4,5* and *pSMXL5*:*SMXL7-GFP smxl3,4,5* are marked by yellow arrows. Bar = 1 cm.

(B) Anthocyanin content in seedlings of wild-type (Col-0), *smxl4,5*, *pSMXL5*:*SMXL5-YFP smxl4,5* #1, *pSMXL5*:*SMAX1-YFP smxl4,5* and *pSMXL5*:*SMXL7-GFP smxl4,5* grown on the 0.5× MS agar with a 16-h-light/8-h-dark photoperiod at 21°C. n = 8 pooled tissue samples. Box-and-whisker plots with the same letter are not significantly different from one another (Student-Newman-Keuls test, $p < 0.05$).

(C) Images of representative 5-day-old seedlings of indicated genotypes in **(B)**. Bar = 1 mm.

Supplemental Figure 3. Verification of SMXL7-GFP, SMXL5-YFP and SMXL5^{mEAR}-YFP expression driven by *SMXL5* promoter in *smxl4,5*.

5 day-old *smxl4,5* root tips of lines carrying *pSMXL7*:*SMXL5-YFP* **(A)**, *pSMXL5*:*SMXL5-YFP* **(B)** and *pSMXL5*:*SMXL5^{mEAR}-YFP* **(C)** transgenes. Shown are overlaps of bright field (grey) and GFP- or YFP- derived signal (yellow). Treatment of 5 µM *rac*-GR24 or mock was applied in **(A)**. Scale Bars represent 50 µm.

Supplemental Figure 4. Root phenotype of plant materials with $GR24^{5DS}$ or KAR_2 treatment in Figure 2A.

Images of representative 9-day-old wild-type (Col-0); *smxl4*,*5*; two independent transgenic lines of *pSMXL5*:*SMXL5-YFP smxl4*,*5*; *pSMXL5*:*SMAX1-YFP smxl4*,*5*; and *pSMXL5*:*SMXL7-GFP smxl4*,*5* plants grown on 0.5× MS agar containing mock (solvent control) ,2 μM $GR24^{5DS}$, 5 μM $GR24^{5DS}$, 2 μM KAR_2, or 5 μM KAR_2. Bar = 10 mm.

Supplemental Figure 5. Overexpression of *SMXL5* increases primary rosette branch number.

(A) Primary rosette branch number of Col-0 and two independent p*35S*:*SMXL5-YFP* transgenic lines at end of proliferative stage (~7-week-old) grown under white light (~110 μmol m^{-2} s^{-1}) with 16-h-light/8-h-dark photoperiod at 21°C. n = 15. Bar = 10 cm.

(B) RT-qPCR analysis of *SMXL5-YFP* transcripts in 7-day-old seedlings of plant materials in **(A)**. *SMXL5-YFP* transcript level is relative to *CACS* internal reference gene transcripts. Bars indicate the mean. n = 3 pooled tissue samples.

Asterisks in **(A)** and **(B)** indicate significant differences compared with Col-0 using Student's t test (*p < 0.05).

Supplemental Figure 6. Knockout of the *SMXL6/7/8* clade in *smxl4,5* causes severe growth defects and lethality.

Rosette phenotypes of 4-week-old wild-type (Col-0) and *smxl4*,*5*,*6*,*7*,*8* grown under a long-day photoperiod (16 h light/8 h dark) are shown.

Supplemental Figure 7. Related to Figure 2. SMXL5 enhances SMXL7 stablity to inhibit *BRC1* promoter activity.

Western blot assay to verify SMXL7 level in the presence or absence of SMXL5 in wild-type tobacco leaves in Figure **2G**. *pBRC1*:*LUC* and *35S*:*SMXL7-FLAG* were co-transformed with empty vector (EV) or *35S*:*SMXL5-YFP*. Proteins were detected by immunoblotting with anti-FLAG or anti-ACTIN monoclonal antibody. ACTIN was used as the loading control. Tobacco leaves solely infiltrated with P19 was used as a negative

control.

Supplemental Figure 8. Time-course of SMXL7 and D14 levels after GR24^{5DS} treatment in Arabidopsis seedlings.

(A) Degradation of SMXL7-GFP protein in wild-type (Col-0), *smxl4*,*5*, and *max2 smxl4*,*5* Arabidopsis seedlings containing p*SMXL7*:*SMXL7-GFP* transgene. Seedlings were treated for 20 minutes after 7 d of growth with 5 μM GR24^{5DS} in 0.5× MS liquid medium. Ponceau-S stainings of Rubisco are used as the loading control. Proteins were detected by immunoblotting with anti-GFP polyclonal antibody. Relative abundances of SMXL7-GFP was determined by densitometry using ImageJ and normalized to respective loading controls, with the zero-time signal set as 1.00.

(B) Degradation of AtD14-CFP protein in wild-type (Col-0), *smxl4*,*5*, and *max2 smxl4*,*5* Arabidopsis seedlings containing *35S*:*AtD14-CFP* transgene. Seedlings were treated for 12 h after 7 d of growth with 5 μM GR24^{5DS} in 0.5× MS liquid medium. Coomassie brilliant blue (CBB) stainings of Rubisco are used as the loading control. Proteins were detected by immunoblotting with anti-GFP polyclonal antibody. Relative abundances of AtD14-CFP was determined by densitometry using ImageJ and normalized to respective loading controls, with the zero-time signal set as 1.00.

Supplemental Figure 9. The EAR motif is important for SMXL5 functions but not interaction with AtD14.

(A) Anthocyanin accumulation in the 5-day-old seedlings of wild-type (Col-0), *smxl4*,*5*, *pSMXL5*:*SMXL5-YFP smxl4*,*5* and *pSMXL5*:*SMXL5*^{mEAR}*-YFP smxl4*,*5*. n = 8 pooled tissue samples. Box-and-whisker plots with the same letter are not significantly different from one another (Student-Newman-Keuls test, $p < 0.05$).

(B) Images of representative 5-day-old seedlings of indicated genotypes in **(A)**. Bar = 1 mm. Data in **(A)** and images in **(B)** of Col-0, *smxl4*,*5*, *pSMXL5*:*SMXL5-YFP smxl4*,*5* are duplicated from Supplemental Figure 2**B** and **C**, respectively, which were done together in the same experiment.

(C) RT-qPCR analysis of *PAP2* gene expression in 7-day-old seedlings of indicated genotypes in **(A)** after 3 h treatment of 5 μM GR24^{5DS} or mock control. *PAP2* transcript level is relative to *CACS* internal reference gene transcripts. Bars indicate the mean. n =

3 pooled tissue samples. Asterisks indicate significant differences to each mock or between compared pairs using Student's t test (*p < 0.05 and **p < 0.01).

(D) The *pBRC1*:*LUC* reporter activity in the presence of SMXL5 or SMXL5^{mEAR} with the co-expression of SMXL7 in wt tobacco are shown. Leaf discs were treated with 10 µM GR24^{5DS} for 3 h. Luminescence is normalized to mCherry internal control. n = 10 leaf discs. Box-and-whisker plots with the same letter are not significantly different from one another (Student-Newman-Keuls test, p < 0.05). Data of EV and SMXL5 is duplicated from Figure **2G**, which was done together in the same experiment.

(E) The *in vitro* GST pull-down of AtD14 and SMXL5 or SMXL5^{mEAR} in the presence or absence of *rac*-GR24. Recombinant proteins were resolved by SDS-PAGE and were visualized via Western blot with anti-His antibody. His-GB1-Atd14^{S97A} with an impaired catalytic triad was used as a negative control. Panels of GST pull-down and input share the same molecular markers. The image of GST pull-down of AtD14 and SMXL5 and the input is duplicated in Figure **6C**.

Supplemental Figure 10. SMAX1$^{\Delta RGKT}$ inhibits the interaction of AtD14 and SMXL7. *N. benthamiana* leaves were transiently co-transformed with *Agrobacterium tumefaciens* strains carrying cLUC-AtD14, SMXL7-nLUC and indicated fusions as well as a strain carrying an mCherry transgene as a transformation control. *35S*:*GFP*, *35S*:*SMXL5*, *35S*:*SMAX1*, *35S*:*SMAX1$^{\Delta RGKT}$*, *35S*:*SMXL7*, or *35S*:*SMXL7$^{\Delta RGKT}$* was co-expressed. Luminescence was measured before and 1 hour after treatment with 10 µM GR24^{5DS}, and was normalized against mCherry fluorescence. n = 12 leaf discs. Box-and-whisker plots with the same letter are not significantly different from one another (Student-Newman-Keuls test, p < 0.05).

Supplemental Table 1. Primers used in this study.

REFERENCES

Aguilar-Martínez, J. A., Poza-Carrión, C., and Cubas, P. (2007). Arabidopsis BRANCHED1 acts as an integrator of branching signals within axillary buds. Plant Cell **19**:458–472.

Blázquez, M. A., Nelson, D. C., and Weijers, D. (2020). Evolution of Plant Hormone Response Pathways. Annu. Rev. Plant Biol. **71**:327–353.

Causier, B., Ashworth, M., Guo, W., Davies, B. (2012). The TOPLESS Interactome: A Framework for Gene Repression in Arabidopsis. *Plant Physiology* **158**: 423-438.

Carbonnel, S., Das, D., Varshney, K., Kolodziej, M. C., Villaécija-Aguilar, J. A., and Gutjahr, C. (2020). The karrikin signaling regulator SMAX1 controls Lotus japonicus root and root hair development by suppressing ethylene biosynthesis. Proc. Natl. Acad. Sci. U. S. A. **117**:21757–21765.

Chen, J., and Shukla, D. (2022). Multiple modes of substrate hydrolysis-induced covalent modification of strigolactone receptors. *bioRxiv* Advance Access published April 22, 2022, doi:10.1101/2022.04.22.489200.

Chen, H., Zou, Y., Shang, Y., Lin, H., Wang, Y., Cai, R., Tang, X., and Zhou, J.-M. (2008). Firefly Luciferase Complementation Imaging Assay for Protein-Protein Interactions in Plants. Plant Physiology **146**:323–324.

Chevalier, F., Nieminen, K., Sánchez-Ferrero, J. C., Rodríguez, M. L., Chagoyen, M., Hardtke, C. S., and Cubas, P. (2014). Strigolactone promotes degradation of DWARF14, an α/β hydrolase essential for strigolactone signaling in Arabidopsis. Plant Cell **26**:1134–1150.

Cho, H., Cho, H. S., Nam, H., Jo, H., Yoon, J., Park, C., Dang, T. V. T., Kim, E., Jeong, J., Park, S., et al. (2018). Translational control of phloem development by RNA G-quadruplex–JULGI determines plant sink strength. Nat. Plants **4**:376–390.

Choi, J., Lee, T., Cho, J., Servante, E. K., Pucker, B., Summers, W., Bowden, S., Rahimi, M., An, K., An, G., et al. (2020). The negative regulator SMAX1 controls mycorrhizal symbiosis and strigolactone biosynthesis in rice. Nat. Commun. **11**:2114.

Clough, S. J., and Bent, A. F. (1998). Floral dip: a simplified method for Agrobacterium-mediated transformation of Arabidopsis thaliana. Plant J. **16**:735–743.

de Saint Germain, A., Clavé, G., Badet-Denisot, M.-A., Pillot, J.-P., Cornu, D., Le Caer, J.-P., Burger, M., Pelissier, F., Retailleau, P., Turnbull, C., et al. (2016). An histidine covalent receptor and butenolide complex mediates strigolactone perception. Nat. Chem. Biol. **12**:787–794.

Fang, Z., Ji, Y., Hu, J., Guo, R., Sun, S., and Wang, X. (2020). Strigolactones and Brassinosteroids Antagonistically Regulate the Stability of the D53–OsBZR1 Complex to Determine FC1 Expression in Rice Tillering. Mol. Plant **13**:586–597.

Feng, Z., Liang, X., Tian, H., Watanabe, Y., Nguyen, K. H., Tran, C. D., Abdelrahman, M., Xu, K., Mostofa, M. G., Van Ha, C., et al. (2023). SUPPRESSOR of MAX2 1 (SMAX1) and SMAX1-LIKE2 (SMXL2) Negatively Regulate Drought Resistance in Arabidopsis thaliana. Plant Cell Physiol. **63**: 1900-1913.

Gietz, R. D., and Woods, R. A. (2002). Transformation of yeast by lithium acetate/single-stranded carrier DNA/polyethylene glycol method. Methods Enzymol. **350**:87–96.

Goddard-Borger, E. D., Ghisalberti, E. L., and Stick, R. V. (2007). Synthesis of the Germination Stimulant 3-Methyl-2H-furo[2,3-c]pyran-2-one and Analogous Compounds from Carbohydrates. ChemInform **38**.

Guillory, A., Lopez-Obando, M., Bouchenine, K., Lambret, L., Le Bris, P., Lécureuil, A., Pillot, J.-P., Steinmetz, V., Boyer, F.-D., Rameau, C., de Saint Germain, A., Bonhomme, S. (2023). *Physcomitrium patens* SMXL homologs are PpMAX2-dependent negative regulators of growth. bioRxiv https://doi.org/10.1101/2023.04.11.536386

Hamiaux, C., Drummond, R. S. M., Janssen, B. J., Ledger, S. E., Cooney, J. M., Newcomb, R. D., and Snowden, K. C. (2012). DAD2 is an α/β hydrolase likely to be involved in the perception of the plant branching hormone, strigolactone. Curr. Biol. **22**:2032–2036.

Hu, J., Ji, Y., Hu, X., Sun, S., and Wang, X. (2020). BES1 Functions as the Co-regulator of D53-like SMXLs to Inhibit BRC1 Expression in Strigolactone-Regulated Shoot Branching in Arabidopsis. Plant Commun. **1**:100014.

Jiang, L., Liu, X., Xiong, G., Liu, H., Chen, F., Wang, L., Meng, X., Liu, G., Yu, H., Yuan, Y., et al. (2013). DWARF 53 acts as a repressor of strigolactone signalling in rice. Nature **504**:401–405.

Ke, J., Ma, H., Gu, X., Thelen, A., Brunzelle, J. S., Li, J., Xu, H. E., and Melcher, K. (2015). Structural basis for recognition of diverse transcriptional repressors by the TOPLESS family of corepressors. Sci. Adv. **1**:e1500107.

Khosla, A., Morffy, N., Li, Q., Faure, L., Chang, S. H., Yao, J., Zheng, J., Cai, M. L., Stanga, J. P., Flematti, G. R., et al. (2020a). Structure-Function Analysis of SMAX1 Reveals Domains that Mediate its Karrikin-Induced Proteolysis and Interaction with the Receptor KAI2. Plant Cell **32**:2639-2659

Khosla, A., Rodriguez-Furlan, C., Kapoor, S., Van Norman, J. M., and Nelson, D. C. (2020b). A series of dual-reporter vectors for ratiometric analysis of protein

abundance in plants. Plant Direct **4**.

Kodama, K., Rich., M. K., Yoda, A., Shimazaki, S., Xie, X., Akiyama, K., Mizuno, Y., Komatsu, A., Luo, Y., Suzuki, H., Kameoka, H., Libourel, C., Keller, J., Sakakibara, K., Nishiyama, T., Nakagawa, T., Mashiguchi, K., Uchida, K., Yoneyama, K., Tanaka, Y., Yamaguchi, S., Shimamura, M., Delaux, P.-M., Nomura, T., Kyozuka, J. (2022). An ancestral function of strigolactones as symbiotic rhizosphere signals. Nature Comm. **13**:3974.

Leydon, A. R., Wang, W., Gala, H. P., Gilmour, S., Juarez-Soli, S., Zahler M. L., Zemke, J. E., Zheng, N., Nemhauser, J. L. (2021). Repression by the Arabidopsis TOPLESS corepressor requires association with the core mediator complex. eLife **10**: e66739.

Li, Q., Martín-Fontecha, E. S., Khosla, A., White, A. R. F., Chang, S., Cubas, P., and Nelson, D. C. (2022). The strigolactone receptor D14 targets SMAX1 for degradation in response to GR24 treatment and osmotic stress. Plant Commun. **3**:100303.

Liang, Y., Ward, S., Li, P., Bennett, T., and Leyser, O. (2016). SMAX1-LIKE7 Signals from the Nucleus to Regulate Shoot Development in Arabidopsis via Partially EAR Motif-Independent Mechanisms. Plant Cell **28**:1581–1601.

Liu, J., Cheng, X., Liu, P., and Sun, J. (2017). miR156-Targeted SBP-Box Transcription Factors Interact with DWARF53 to Regulate TEOSINTE BRANCHED1 and BARREN STALK1 Expression in Bread Wheat. Plant Physiol. **174**:1931–1948.

Lopez-Obando, M., Guillory, A., Boyer, F.-D., Cornu, D., Hoffmann, B., Le Bris, P., Pouvreau, J.-B., Delavault, P., Rameau, C., de Saint Germain, A., Bonhomme, S. (2021). The *Physcomitrium* (*Physcomitrella*) *patens* PpKAI2L receptors for strigolactones and related compounds function via MAX2-dependent and -independent pathways. Plant Cell **33**:3487-3512.

Ma, H., Duan, J., Ke, J., He, Y., Gu, X., Xu, T.-H., Yu, H., Wang, Y., Brunzelle, J. S., Jiang, Y., et al. (2017). A D53 repression motif induces oligomerization of TOPLESS corepressors and promotes assembly of a corepressor-nucleosome complex. Sci. Adv. **3**:e1601217.

Mizuno, Y., Komatsu, A., Shimazaki, S., Naramoto, S., Inoue, K., Xie, X., Ishizaki, K., Kohchi, T., Kyozuka, J. (2021). Major components of the KARRIKIN INSENSITIVE2-dependent signaling pathway are conserved in the liverwort *Marchantia polymorpha*. Plant Cell **33**:2395-2411.

Nelson, D. C. (2021). The mechanism of host-induced germination in root parasitic plants. Plant Physiol. **185**:1353-1373.

Patil, S. B., Barbier, F. F., Zhao, J., Zafar, S. A., Uzair, M., Sun, Y., Fang, J., Perez-

Garcia, M.-D., Bertheloot, J., Sakr, S., et al. (2022). Sucrose promotes D53 accumulation and tillering in rice. New Phytol. **234**:122–136.

Plant, A. R., Larrieu, A., Causier, B. (2021). Repressor for hire! The vital roles of TOPLESS-mediated transcriptional repression in plants. New Phytol. **231**: 963–973.

Scaffidi, A., Waters, M. T., Sun, Y. K., Skelton, B. W., Dixon, K. W., Ghisalberti, E. L., Flematti, G. R., and Smith, S. M. (2014). Strigolactone Hormones and Their Stereoisomers Signal through Two Related Receptor Proteins to Induce Different Physiological Responses in Arabidopsis. Plant Physiol. **165**:1221–1232.

Song, X., Lu, Z., Yu, H., Shao, G., Xiong, J., Meng, X., Jing, Y., Liu, G., Xiong, G., Duan, J., et al. (2017). IPA1 functions as a downstream transcription factor repressed by D53 in strigolactone signaling in rice. Cell Res. **27**:1128–1141.

Soundappan, I., Bennett, T., Morffy, N., Liang, Y., Stanga, J. P., Abbas, A., Leyser, O., and Nelson, D. C. (2015). SMAX1-LIKE/D53 Family Members Enable Distinct MAX2-Dependent Responses to Strigolactones and Karrikins in Arabidopsis. Plant Cell **27**:3143–3159.

Stanga, J. P., Smith, S. M., Briggs, W. R., and Nelson, D. C. (2013). SUPPRESSOR OF MORE AXILLARY GROWTH2 1 controls seed germination and seedling development in Arabidopsis. Plant Physiol. **163**:318–330.

Stanga, J. P., Morffy, N., and Nelson, D. C. (2016). Functional redundancy in the control of seedling growth by the karrikin signaling pathway. Planta **243**:1397–1406.

Sun, H., Guo, X., Qi, X., Feng, F., Xie, X., Zhang, Y., and Zhao, Q. (2021). SPL14/17 act downstream of strigolactone signalling to modulate rice root elongation in response to nitrate supply. Plant J. **106**:649–660.

Tal, L., Palayam, M., Ron, M., Young, A., Britt, A., and Shabek, N. (2022). A conformational switch in the SCF-D3/MAX2 ubiquitin ligase facilitates strigolactone signalling. Nat. Plants **8**:561–573.

Temmerman, A., Guillory, A., Bonhomme, S., Goormachtig, S., and Struk, S. (2022). Masks Start to Drop: Suppressor of MAX2 1-Like Proteins Reveal Their Many Faces. Front. Plant Sci. **13**:887232.

Villaécija-Aguilar, J. A., Hamon-Josse, M., Carbonnel, S., Kretschmar, A., Schmid, C., Dawid, C., Bennett, T., and Gutjahr, C. (2019). SMAX1/SMXL2 regulate root and root hair development downstream of KAI2-mediated signalling in Arabidopsis. PLOS Genet. **15**:e1008327.

Walker, C. H., Siu-Ting, K., Taylor, A., O'Connell, M. J., and Bennett, T. (2019). Strigolactone synthesis is ancestral in land plants, but canonical strigolactone

signalling is a flowering plant innovation. BMC Biol. **17**:70.

Wallner, E.-S., López-Salmerón, V., Belevich, I., Poschet, G., Jung, I., Grünwald, K., Sevilem, I., Jokitalo, E., Hell, R., Helariutta, Y., et al. (2017). Strigolactone- and Karrikin-Independent SMXL Proteins Are Central Regulators of Phloem Formation. Curr. Biol. **27**:1241–1247.

Wallner, E., Tonn, N., Shi, D., Jouannet, V., and Greb, T. (2020). *SUPPRESSOR OF MAX2 1-LIKE 5* promotes secondary phloem formation during radial stem growth. Plant J. **102**:903–915.

Wallner, E.-S., Tonn, N., Shi, D., Luzzietti, L., Wanke, F., Hunziker, P., Xu, Y., Jung, I., Lopéz-Salmerón, V., Gebert, M., Wenzl, C., Lohmann, J.U., Harter, K., and Greb, T. (2023) OBERON3 and SUPPRESSOR OF MAX2 1-LIKE proteins form a regulatory module driving phloem development. Nat. Commun. **14**: 2128

Wang, L., Wang, B., Jiang, L., Liu, X., Li, X., Lu, Z., Meng, X., Wang, Y., Smith, S. M., and Li, J. (2015). Strigolactone Signaling in Arabidopsis Regulates Shoot Development by Targeting D53-Like SMXL Repressor Proteins for Ubiquitination and Degradation. Plant Cell **27**:3128–3142.

Wang, L., Xu, Q., Yu, H., Ma, H., Li, X., Yang, J., Chu, J., Xie, Q., Wang, Y., Smith, S. M., et al. (2020a). Strigolactone and Karrikin Signaling Pathways Elicit Ubiquitination and Proteolysis of SMXL2 to Regulate Hypocotyl Elongation in Arabidopsis. Plant Cell **32**:2251–2270.

Wang, L., Wang, B., Yu, H., Guo, H., Lin, T., Kou, L., Wang, A., Shao, N., Ma, H., Xiong, G., et al. (2020b). Transcriptional regulation of strigolactone signalling in Arabidopsis. Nature **583**:277–281.

Waters, M. T., Nelson, D. C. (2023). Karrikin perception and signalling. New Phytologist **237**: 1525-1541.

Waters, M. T., Nelson, D. C., Scaffidi, A., Flematti, G. R., Sun, Y. K., Dixon, K. W., and Smith, S. M. (2012). Specialisation within the DWARF14 protein family confers distinct responses to karrikins and strigolactones in Arabidopsis. Development **139**:1285–1295.

Waters, M. T., Scaffidi, A., Moulin, S. L. Y., Sun, Y. K., Flematti, G. R., and Smith, S. M. (2015). A Selaginella moellendorffii Ortholog of KARRIKIN INSENSITIVE2 Functions in Arabidopsis Development but Cannot Mediate Responses to Karrikins or Strigolactones. Plant Cell **27**:1925–1944.

Waters, M. T., Gutjahr, C., Bennett, T., and Nelson, D. C. (2017). Strigolactone Signaling and Evolution. Annu. Rev. Plant Biol. **68**:291–322.

White, A. R. F., Mendez, J. A., Khosla, A., and Nelson, D. C. (2022). Rapid analysis of strigolactone receptor activity in a *Nicotiana benthamiana dwarf14* mutant. Plant

Direct **6**: e389

Xie, Y., Liu, Y., Ma, M., Zhou, Q., Zhao, Y., Zhao, B., Wang, B., Wei, H., and Wang, H. (2020). Arabidopsis FHY3 and FAR1 integrate light and strigolactone signaling to regulate branching. Nat. Commun. **11**:1955.

Yang, T., Zhang, L., Hao, H., Zhang, P., Zhu, H., Cheng, W., Wang, Y., Wang, X., and Wang, C. (2015). Nuclear-localized AtHSPR links abscisic acid-dependent salt tolerance and antioxidant defense in Arabidopsis. Plant J. **84**:1274–1294.

Yang, T., Sun, Y., Wang, Y., Zhou, L., Chen, M., Bian, Z., Lian, Y., Xuan, L., Yuan, G., Wang, X., et al. (2020). AtHSPR is involved in GA- and light intensity-mediated control of flowering time and seed set in Arabidopsis. J. Exp. Bot. **71**:3543–3559.

Yao, R., Ming, Z., Yan, L., Li, S., Wang, F., Ma, S., Yu, C., Yang, M., Chen, L., Chen, L., et al. (2016). DWARF14 is a non-canonical hormone receptor for strigolactone. Nature **536**:469–473.

Yao, R., Wang, L., Li, Y., Chen, L., Li, S., Du, X., Wang, B., Yan, J., Li, J., and Xie, D. (2018). Rice DWARF14 acts as an unconventional hormone receptor for strigolactone. J. Exp. Bot. **69**:2355-2365.

Yoo, S. D., Cho, Y. H., & Sheen, J. (2007). Arabidopsis mesophyll protoplasts: a versatile cell system for transient gene expression analysis. Nat. Protoc. **2**:1565–1572.

Zheng, J., Hong, K., Zeng, L., Wang, L., Kang, S., Qu, M., Dai, J., Zou, L., Zhu, L., Tang, Z., et al. (2020). Karrikin Signaling Acts Parallel to and Additively with Strigolactone Signaling to Regulate Rice Mesocotyl Elongation in Darkness. Plant Cell **32**:2780–2805.

Zhou, F., Lin, Q., Zhu, L., Ren, Y., Zhou, K., Shabek, N., Wu, F., Mao, H., Dong, W., Gan, L., et al. (2013). D14-SCF(D3)-dependent degradation of D53 regulates strigolactone signalling. Nature **504**:406–410.

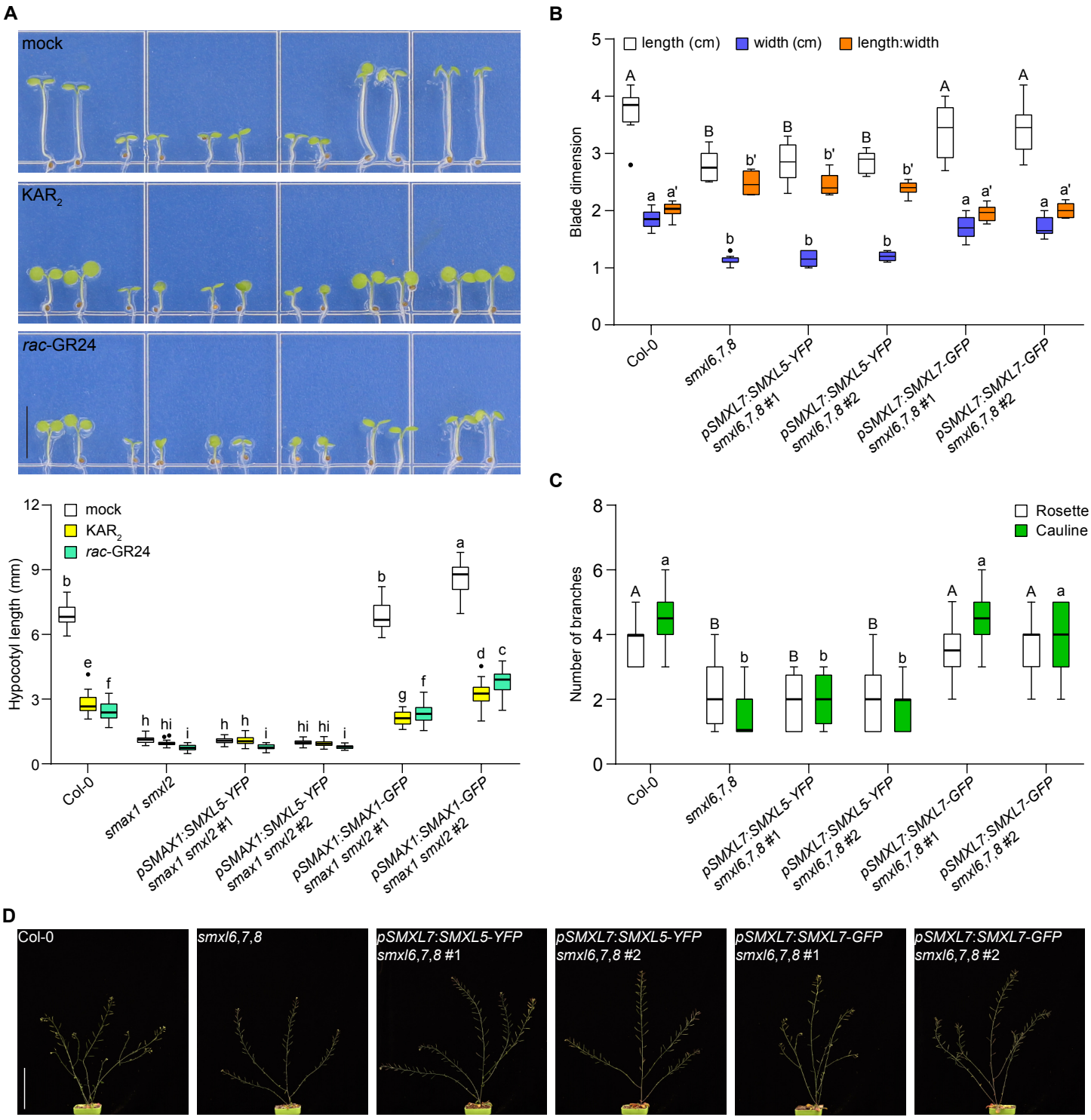

Figure 1. SMXL5 cannot functionally replace SMXL proteins of other clades.
(A) Hypocotyl lengths of 5-day-old seedlings of Col-0, *smax1 smxl2*, two independent *pSMAX1*:*SMXL5-YFP smax1 smxl2* transgenic lines and two independent *pSMAX1*:*SMAX1-GFP smax1 smxl2* transgenic lines grown under continuous red light for 4 days on 0.5× MS medium containing 1 μM KAR_2, 1 μM *rac*-GR24, or mock control. Bar = 5 mm.
(B) Blade length (white), not including the petiole, width (blue) and length:width ratio (orange) of the 7th leaf of 35-day-old Col-0, *smxl6,7,8*, two independent *pSMXL7*:*SMXL5-YFP smxl6,7,8* transgenic plants and two independent *pSMXL7*:*SMXL7-GFP smxl6,7,8* transgenic plants.
(C) Number of rosette and cauline branches of plants in **(B)**.
(D) Adult shoot morphology of plants in **(C)**. Bar = 10 cm.
Box-and-whisker plots in **(A)**, **(B)**, and **(C)** with the same letter are not significantly different from one another (Student-Newman-Keuls test, $p < 0.05$). Lowercase, uppercase and single quotation marks differentiate statistical tests of measurements.

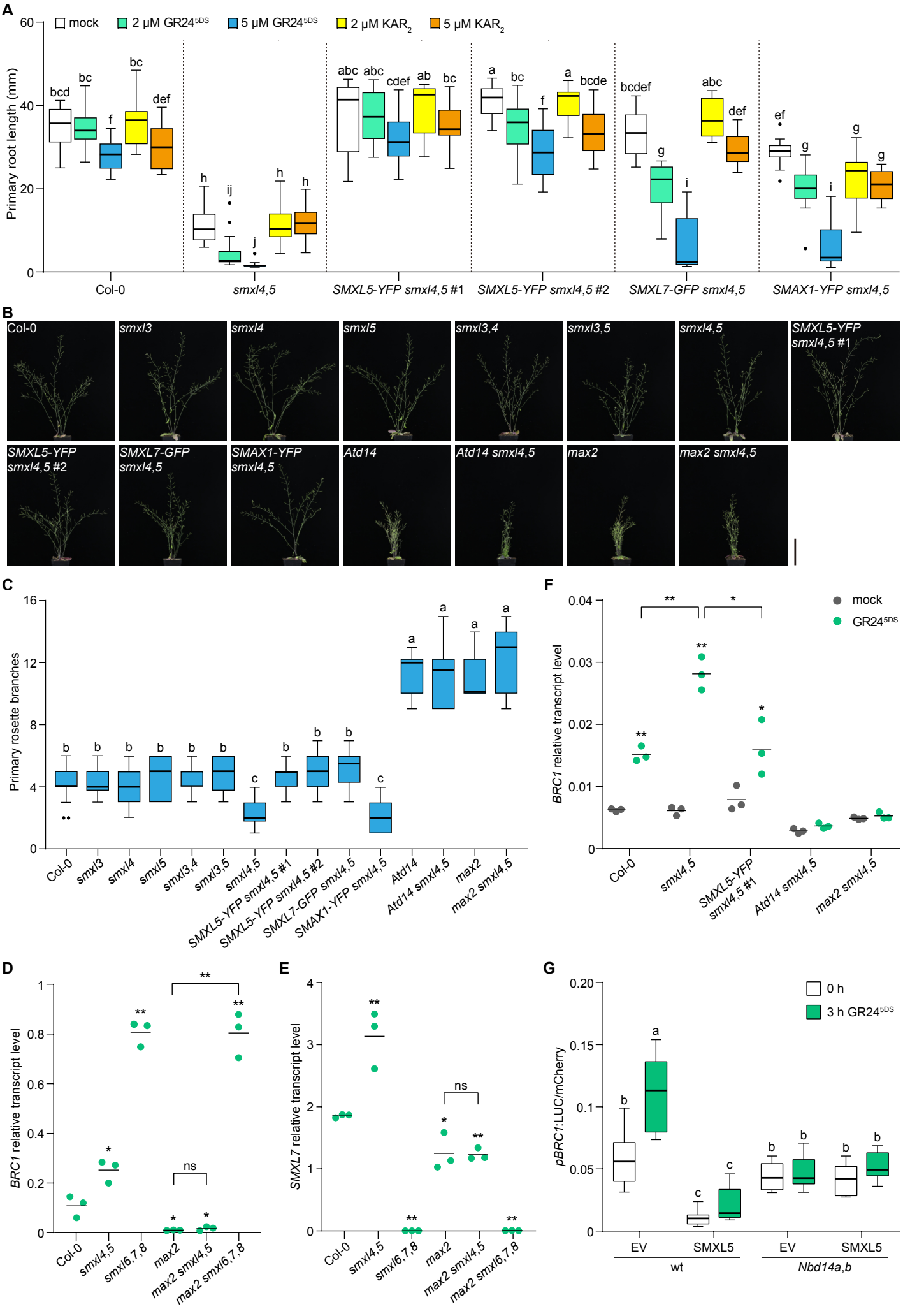
A
mock
2 µM GR24^5DS
5 µM GR24^5DS
2 µM KAR2
5 µM KAR2
Primary root length (mm)
Col-0
smxl4,5
SMXL5-YFP smxl4,5 #1
SMXL5-YFP smxl4,5 #2
SMXL7-GFP smxl4,5
SMAX1-YFP smxl4,5
B
Col-0
smxl3
smxl4
smxl5
smxl3,4
smxl3,5
smxl4,5
SMXL5-YFP smxl4,5 #1
SMXL5-YFP smxl4,5 #2
SMXL7-GFP smxl4,5
SMAX1-YFP smxl4,5
Atd14
Atd14 smxl4,5
max2
max2 smxl4,5
C
Primary rosette branches
F
BRC1 relative transcript level
mock
GR24^5DS
D
BRC1 relative transcript level
ns
E
SMXL7 relative transcript level
ns
G
pBRC1:LUC/mCherry
0 h
3 h GR24^5DS
EV
SMXL5
wt
Nbd14a,b

Figure 2. Loss of *SMXL4* and *SMXL5* enhances strigolactone responses.

(A) Primary root lengths of 9-day-old wild-type (Col-0); *smxl4*,*5*; two independent transgenic lines of *pSMXL5*:*SMXL5-YFP smxl4*,*5*; *pSMXL5*:*SMAX1-YFP smxl4*,*5*; and *pSMXL5*:*SMXL7-GFP smxl4*,*5* plants grown on 0.5× MS agar containing mock (solvent control), 2 μM $GR24^{5DS}$, 5 μM $GR24^{5DS}$, 2 μM KAR_2 or 5 μM KAR_2. n = 14-20.

(B) Adult shoot morphology of wild-type (Col-0); *smxl3*; *smxl4*; *smxl5*; *smxl3*,*4*; *smxl3*,*5*; *smxl4*,*5*; two independent transgenic lines of *pSMXL5*:*SMXL5-YFP smxl4*,*5*; *pSMXL5*:*SMAX1-YFP smxl4*,*5*; *pSMXL5*:*SMXL7-GFP smxl4*,*5*; *Atd14*; *Atd14 smxl4*,*5*; *max2*; and *max2 smxl4*,*5* at the proliferative stage (~7-week-old) grown under white light (~110 μmol m^{-2} s^{-1}) with 16-h-light/8-h-dark photoperiod at 21°C. Bar = 10 cm.

(C) Primary rosette branch number of indicated genotypes shown in **(B)**. n = 10-15.

(D) RT-qPCR analysis of *BRC1* gene expression in nonelongated axillary buds of Col-0, *smxl4*,*5*, *smxl6*,*7*,*8*, *max2 smxl4*,*5*, and *max2 smxl6*,*7*,*8*. *BRC1* transcript level is relative to *CACS* internal reference gene transcripts.

(E) RT-qPCR analysis of *SMXL7* gene expression in nonelongated axillary buds of Col-0, *smxl4*,*5*, *smxl6*,*7*,*8*, *max2 smxl4*,*5*, and *max2 smxl6*,*7*,*8*. *SMXL7* transcript level is relative to *CACS* internal reference gene transcripts.

(F) RT-qPCR analysis of *BRC1* transcripts in 7-day-old seedlings of Col-0; *smxl4*,*5*; *pSMXL5*:*SMXL5 smxl4*,*5*; *Atd14 smxl4*,*5*; and *max2 smxl4*,*5* after 3 h treatment with 5 μM $GR24^{5DS}$ or mock control. *BRC1* transcript level is relative to *CACS* internal reference gene transcripts.

(G) The *pBRC1*:*LUC* reporter activity with the presence or absence of SMXL5 in wt tobacco and *Nbd14a*,*b*. SMXL7 was co-expressed. Leaf discs were treated with 10 μM $GR24^{5DS}$ for 3 h. Luminescence was normalized to mCherry internal control. n = 10 leaf discs.

Bars in **(D)**, **(E)** and **(F)** indicate the mean. n = 3 pooled tissue samples. Asterisks in **(D)**, **(E)** and **(F)** indicate significant differences between mock and treated samples within genotype using Student's t test (*$p < 0.05$ or **$p < 0.01$; ns indicates no significance).

Box-and-whisker plots in **(A)**, **(C)** and **(G)** with the same letter are not significantly different from one another (Student-Newman-Keuls test, $p < 0.05$).

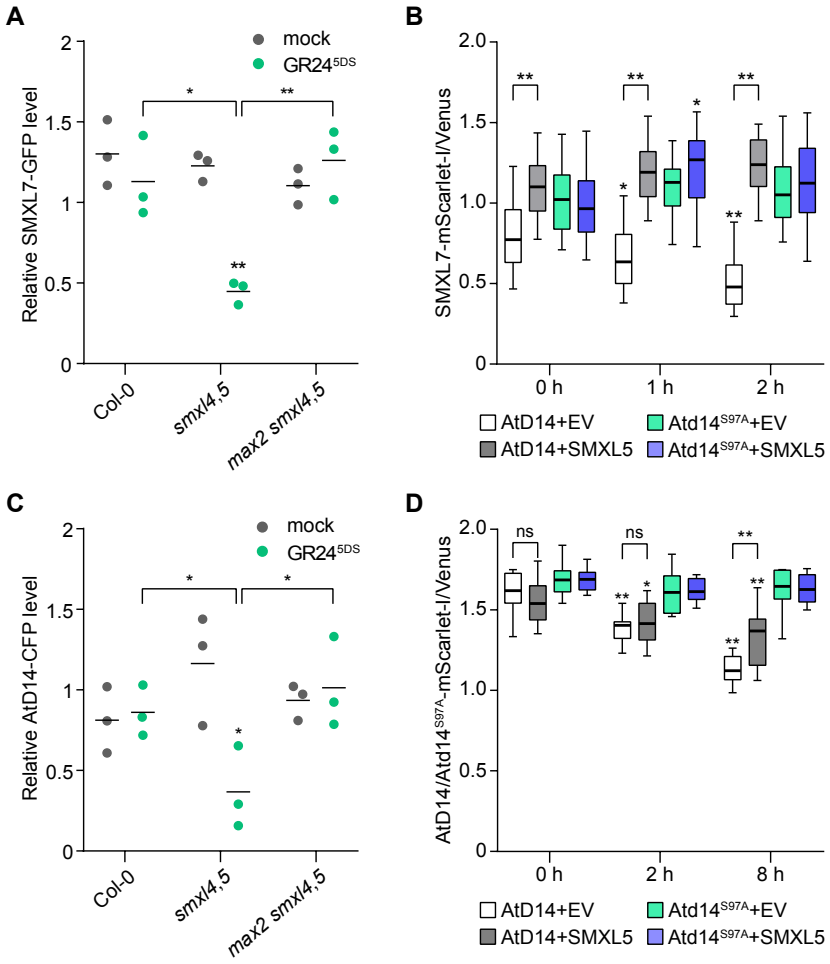

Figure 3. SMXL4 and SMXL5 attenuate GR24^{5DS}-induced degradation of SMXL7 and AtD14.
(A) Relative abundance of SMXL7-GFP in Col-0, *smxl4,5* and *max2 smxl4,5* after 5 min treatment of 5 µM GR24^{5DS} or mock control determined by Western blot densitometry of blot shown in Supplemental Figure **8A**.
(B) Time course assay of SMXL7 stability in *N. benthamiana* under 10 µM GR24^{5DS} treatment. Relative fluorescence from the SMXL7-mScarlet-I reporter with the presence or absence of SMXL5 after co-expressing AtD14 or Atd14^{S97A} in *Nbd14a,b* is shown. n = 18 leaf discs. Asterisks indicate significant differences to each group at 0 h using Student's t test (*p < 0.05 and **p < 0.01).
(C) Relative abundance of AtD14-CFP in Col-0, *smxl4,5* and *max2 smxl4,5* after 4 h treatment of 5 µM GR24^{5DS} or mock control determined by Western blot densitometry of blot shown in Supplemental Figure **8C**.
(D) Time course assay of AtD14 and Atd14^{S97A} stability in *N. benthamiana* under 10 µM GR24^{5DS} treatment. Relative fluorescence from the AtD14-mScarlet-I reporter and Atd14^{S97A}-mScarlet-I reporter after co-expressing an empty vector (EV) or SMXL5 in *Nbd14a,b* is shown. n = 10 leaf discs. Asterisks indicate significant differences to each group at 0 h or between compared pairs using the Student's t test (*p < 0.05 and **p < 0.01; ns indicates no significance).
Relative abundance of SMXL7-GFP in **(A)** and AtD14-CFP in **(C)** determined by densitometry was normalized to respective loading controls, with the zero-time signal set as 1.00. n = 3 experimental replicates (three independently prepared genotype-treatment protein samples analyzed on separate immunoblots). Bars indicate the mean. Asterisks indicate significant differences to each mock or between compared pairs using Student's t test (*p < 0.05 and **p < 0.01).

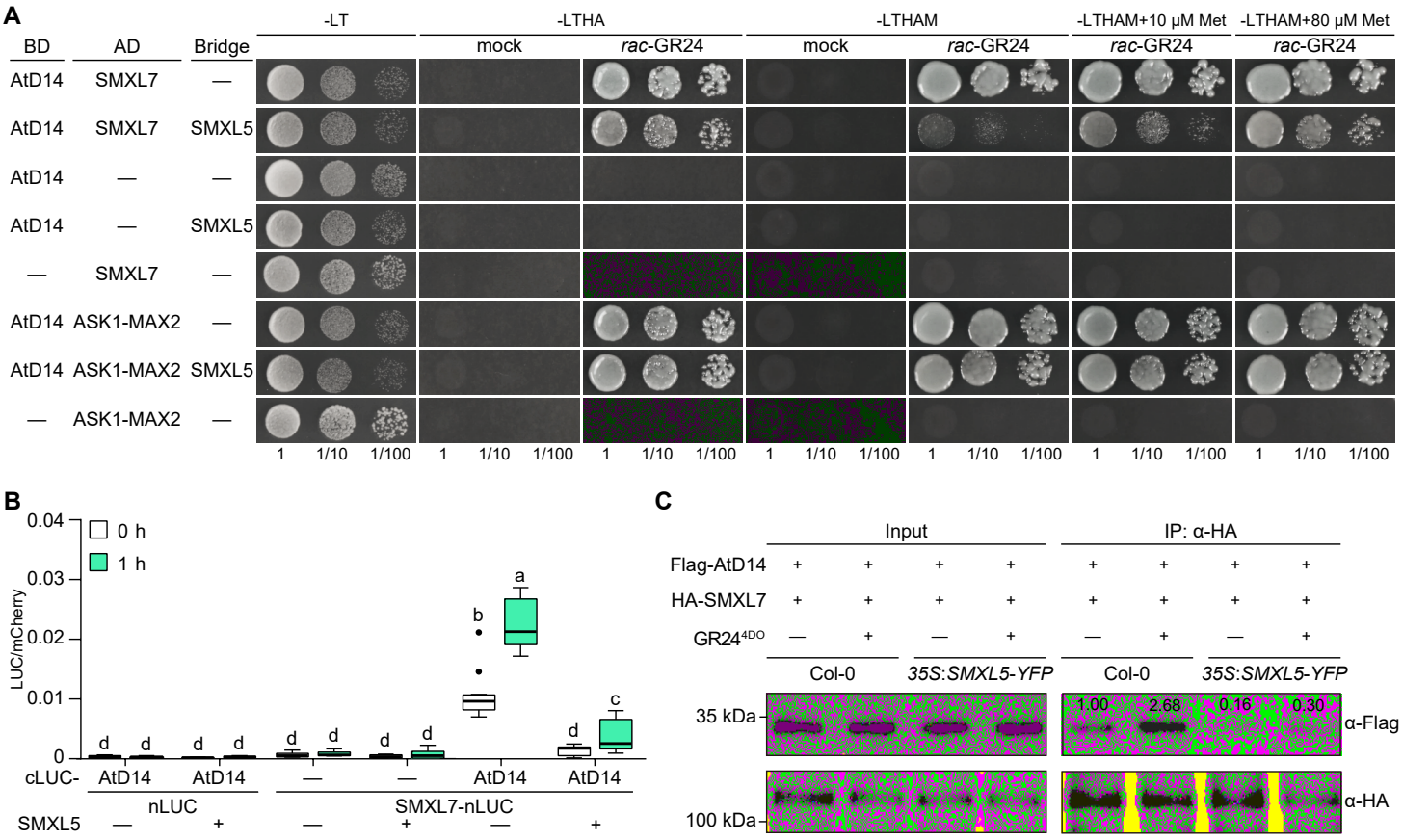

Figure 4. SMXL5 inhibits AtD14-SMXL7 association.
(A) Yeast three-hybrid assay of AtD14-SMXL7 or AtD14-ASK1-MAX2 interaction in the absence or presence of SMXL5. AtD14 was fused to GAL4-BD. SMXL7 and ASK1-MAX2 were fused to GAL4-AD. *SMXL5* expression was driven by the *MET25* promoter. Serial 10-fold dilutions of yeast cultures starting from OD_{600} 2.5 were spotted onto selective growth medium (-L, -Leu; -T, -Trp; -H, -His; -A, -Ade; -M, -Met) that was supplemented with 5 µM *rac*-GR24 or mock control. Methionine was re-supplemented into -LTHAM medium as indicated to suppress the *MET25* promoter activity.
(B) Effect of SMXL5 on interaction of AtD14 and SMXL7 was detected in the split-luciferase complementation assay. *N. benthamiana* leaves were transiently co-transformed with *Agrobacterium tumefaciens* strains carrying cLUC, nLUC, or indicated fusions as well as a strain carrying an mCherry transgene as a transformation control. + and – indicate *35S*:*SMXL5-YFP* and *35S*:*GFP*, respectively. Luminescence was measured before and 1 hour after treatment with 10 µM $GR24^{5DS}$, and was normalized against mCherry fluorescence. n = 10-12 leaf discs. Box-and-whisker plots with the same letter are not significantly different from one another (Student-Newman-Keuls test, $p < 0.05$).
(C) Association of Flag-AtD14 with HA-SMXL7 revealed by Co-IP assay (IP) in protoplasts of wild-type (Col-0) or *35S*:*SMXL5-YFP* transgenic plants in the absence or presence of 100 µM $GR24^{4DO}$. The Flag-AtD14 and HA-SMXL7 fusion proteins were detected with anti-Flag monoclonal antibody and anti-HA monoclonal antibody, respectively. Relative abundances of Flag-AtD14 after immunoprecipitation were determined by densitometry with the signal from Col-0 protoplasts in the absence of $GR24^{4DO}$ set as 1.00.

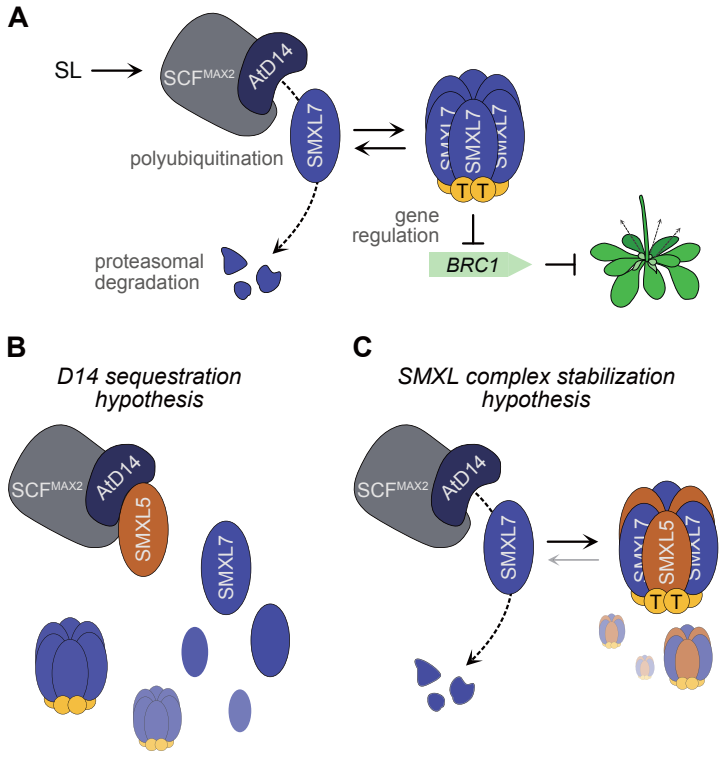

Figure 5. Two hypotheses of how SMXL5 attenuates strigolactone signaling.

(A) A model of strigolactone signaling. After binding and/or hydrolysis of strigolactone, AtD14 associates with SCF^{MAX2} and target proteins such as SMXL7. The target(s) are polyubiquitinated and then destroyed by the 26S proteasome, relieving transcriptional repression by SMXL proteins. We propose that SMXL proteins form multimeric complexes (here shown as a hexamer) that can also dissociate into monomers. SMXL proteins can interact with TPL/TPR (yellow, "T") via a C-terminal EAR motif, which can promote the formation or stability of SMXL multimers (Ma et al., 2017). TPL/TPR proteins are known to impose transcriptional repression through interaction with histone deacetylases, the Mediator complex, and/or histone proteins (not depicted). SMXL proteins may bind DNA directly or indirectly through interaction with transcription factors (not depicted). *BRC1* is shown as an example of a downstream transcriptional target of SMXL7. *BRC1* inhibits axillary bud outgrowth (branching). It is not yet known whether SMXL proteins function as transcriptional corepressors with TPL/TPR in monomeric and/or multimeric states. It is also unknown whether AtD14-SCF^{MAX2} targets SMXL protein monomers, multimers, or both. As drawn, this cartoon proposes that SMXL monomers are targeted for degradation and SMXL multimers regulate gene expression.

(B) The D14 sequestration hypothesis proposes that SMXL5, which is resistant to MAX2-dependent degradation, forms non-productive interactions with AtD14-SCF^{MAX2} that competitively interfere with AtD14-SCF^{MAX2} targeting of SMXL7. This results in an increase in SMXL7 abundance and reduced SL responses.

(C) The SMXL complex stabilization hypothesis proposes that SMXL7 is somehow less susceptible to targeting by AtD14-SCF^{MAX2} when it forms heteromeric complexes with SMXL5. For example, SMXL5 might promote multimer formation or reduce multimer dissociation, causing an equilibrium shift toward multimeric SMXL7 and increased SMXL7 abundance.

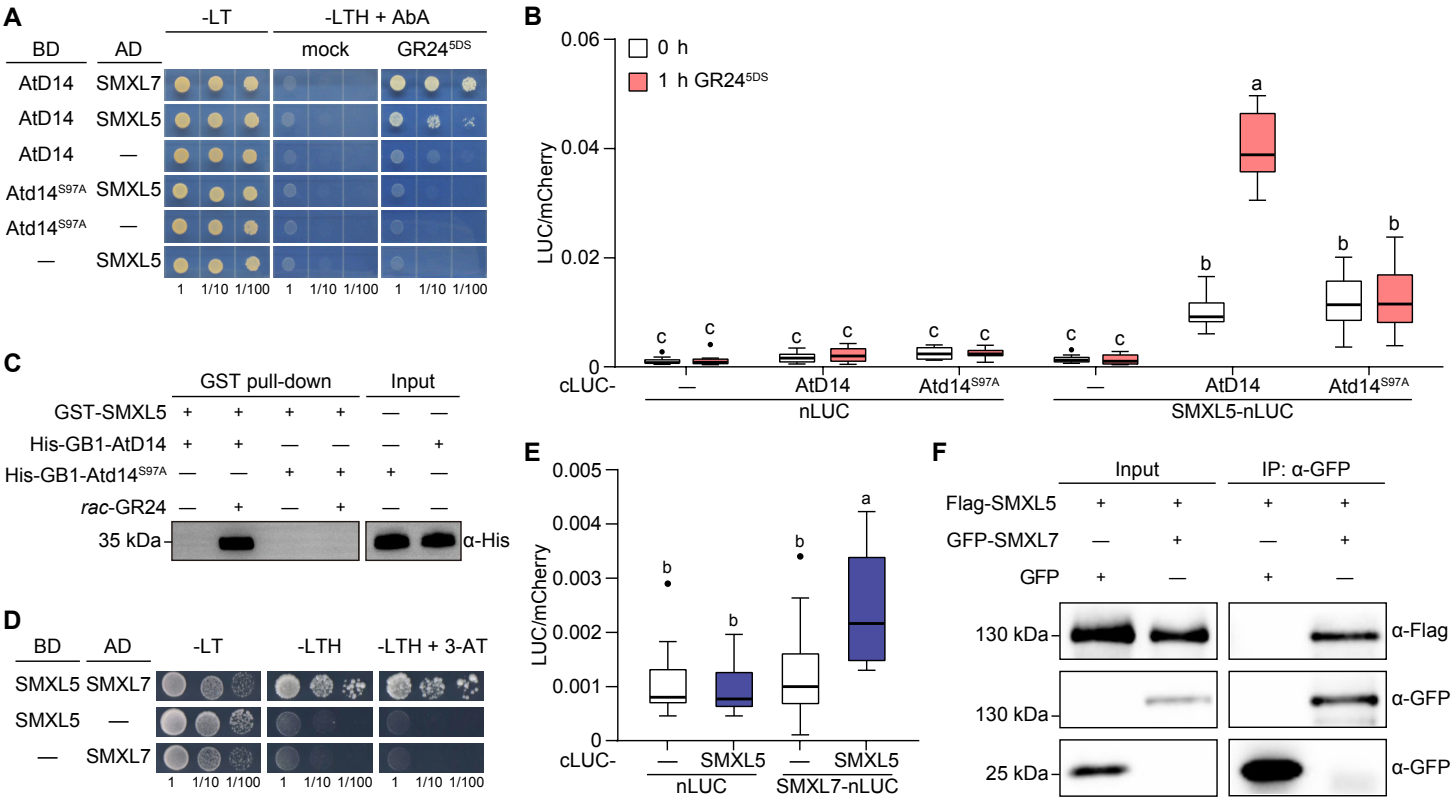

Figure 6. SMXL5 physically interacts with AtD14 and SMXL7.

(A) Yeast two-hybrid assays of SMXL5 interactions with AtD14 and Atd14^{S97A} using yeast strain Y2HGold. AtD14 and Atd14^{S97A} were fused to GAL4-BD. SMXL5 and SMXL7 were fused to GAL4-AD. 100 ng/mL Aureobasidin A (AbA) was added into -LTH medium for more stringent selection. Serial 10-fold dilutions of yeast cultures starting from OD_{600} 1.0 were spotted onto selective growth medium supplemented with 2 μM GR24^{5DS} or mock control.

(B) Split-luciferase complementation assay for SMXL5 interactions with AtD14 and Atd14^{S97A}. Luminescence was measured before and 1 hour after treatment with 10 μM GR24^{5DS}, and was normalized against mCherry fluorescence. n ≥ 12 leaf discs.

(C) The *in vitro* GST pull-down assay of GST-SMXL5 and His-GB1-AtD14 or His-GB1-Atd14^{S97A} in the presence or absence of *rac*-GR24. Recombinant proteins were resolved by SDS-PAGE and were visualized via Western blot with anti-His antibody. Panels of GST pull-down and input share the same molecular markers.

(D) Yeast two-hybrid assays for investigating heterodimerization or homodimerization of SMXL5 and SMXL7. 0.1 mM 3-Amino-1,2,4-triazole (3-AT) was added to -LTH medium to reduce background growth. Serial 10-fold dilutions of yeast cultures starting from OD_{600} 2.5 were spotted onto selective growth medium.

(E) Split-luciferase complementation assay for SMXL5 interaction with SMXL7. n = 10-15 leaf discs.

(F) Association of Flag-SMXL5 with GFP-SMXL7 revealed by Co-IP assay (IP) in protoplasts of wild-type (Col-0) in the absence or presence of 100 μM GR24^{4DO}. The Flag-SMXL5 fusion protein was detected with anti-Flag monoclonal antibody; the GFP-SMXL7 fusion protein and GFP were detected with anti-GFP monoclonal antibody.

Box-and-whisker plots in **(B)** and **(E)** with the same letter are not significantly different from one another (Student-Newman-Keuls test, $p < 0.05$).

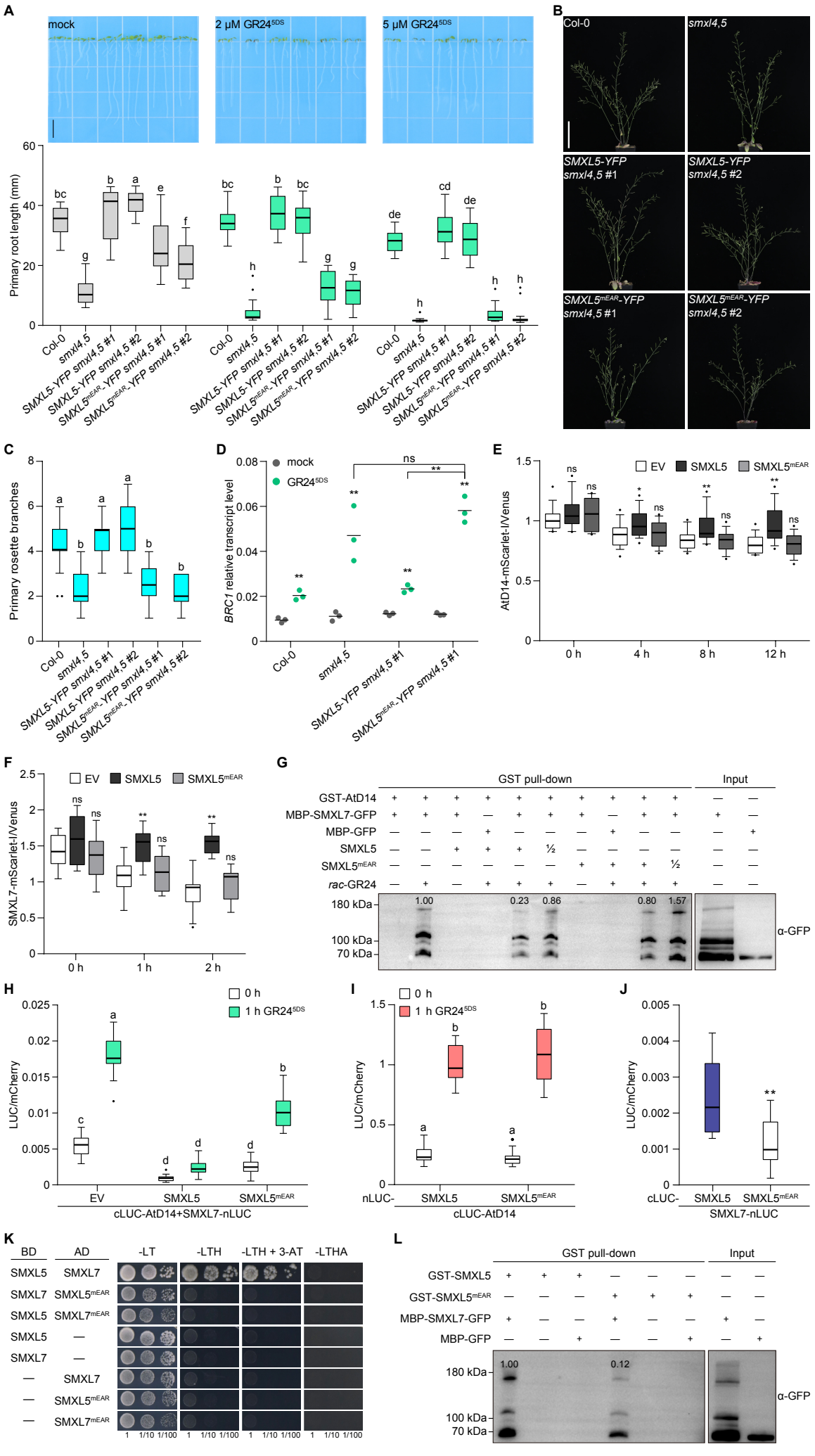
A
mock
2 µM GR24^5DS
5 µM GR24^5DS
Primary root length (mm)
Col-0
smxl4,5
SMXL5-YFP smxl4,5 #1
SMXL5-YFP smxl4,5 #2
SMXL5^mEAR-YFP smxl4,5 #1
SMXL5^mEAR-YFP smxl4,5 #2
B
Col-0
smxl4,5
SMXL5-YFP smxl4,5 #1
SMXL5-YFP smxl4,5 #2
SMXL5^mEAR-YFP smxl4,5 #1
SMXL5^mEAR-YFP smxl4,5 #2
C
Primary rosette branches
D
mock
GR24^5DS
BRC1 relative transcript level
E
EV
SMXL5
SMXL5^mEAR
AtD14-mScarlet-I/Venus
0 h
4 h
8 h
12 h
F
SMXL7-mScarlet-I/Venus
0 h
1 h
2 h
G
GST pull-down
Input
GST-AtD14
MBP-SMXL7-GFP
MBP-GFP
SMXL5
SMXL5^mEAR
rac-GR24
180 kDa
100 kDa
70 kDa
α-GFP
H
0 h
1 h GR24^5DS
LUC/mCherry
EV
SMXL5
SMXL5^mEAR
cLUC-AtD14+SMXL7-nLUC
I
nLUC-
cLUC-AtD14
J
cLUC-
SMXL7-nLUC
K
BD
AD
-LT
-LTH
-LTH + 3-AT
-LTHA
SMXL5
SMXL7
SMXL7^mEAR
1
1/10
1/100
L
GST-SMXL5
GST-SMXL5^mEAR
MBP-SMXL7-GFP
MBP-GFP

Figure 7. Attenuation of SL signaling by SMXL5 requires the EAR motif.

(A) Root lengths of 9-day-old wild-type (Col-0); *smxl4*,*5*; two independent transgenic lines of *pSMXL5*:*SMXL5-YFP smxl4*,*5*; and two independent transgenic lines of *pSMXL5*:*SMXL5*^{mEAR}*-YFP smxl4*,*5* (SMXL5 variant with a mutated EAR motif, sequence LDLNI modified to ADANA) plants grown on the 0.5× MS agar containing mock, 2 μM GR24^{5DS} or 5 μM GR24^{5DS}. n = 16-20. Bar = 10 mm. Images and data of wild-type (Col-0); *smxl4*,*5*; and two independent transgenic lines of *pSMXL5*:*SMXL5-YFP smxl4*,*5* are duplicated in Supplemental Figure 4 and Figure **2A**, respectively, which were done together in the same experiment.

(B) Adult shoot morphology of wild-type (Col-0); *smxl4*,*5*; two independent transgenic lines of *pSMXL5*:*SMXL5-YFP smxl4*,*5*; and two independent transgenic lines of *pSMXL5*:*SMXL5*^{mEAR}*-YFP smxl4*,*5* at the proliferative stage (~7-week-old) grown under white light (~110 μmol m^{-2} s^{-1}) with 16-h-light/8-h-dark photoperiod at 21°C. Bar = 10 cm.

(C) Primary rosette branch number of indicated genotypes shown in **(B)**. n = 10-15.

(D) RT-qPCR analysis of *BRC1* gene expression in 7-day-old seedlings of wild-type (Col-0); *smxl4*,*5*; *pSMXL5*:*SMXL5-YFP smxl4*,*5* #1; and *pSMXL5*:*SMXL5*^{mEAR}*-YFP smxl4*,*5* #1 after 3 h treatment of 5 μM GR24^{5DS} or mock control. *BRC1* transcript level is relative to *CACS* internal reference gene transcripts. Bars indicate the mean. n = 3 pooled tissue samples. Asterisks indicate significant differences to each mock or between compared pairs using Student's t test (**p < 0.01; ns indicates no significance).

(E) Time course assay of AtD14 stability in *N. benthamiana* under 10 μM GR24^{5DS} treatment. Relative fluorescence from the AtD14-mScarlet-I reporter with SMXL5 or SMXL5^{mEAR} in wt tobacco is shown. n = 17 leaf discs.

(F) Time course assay of SMXL7 stability in *N. benthamiana* under 10 μM GR24^{5DS} treatment. Relative fluorescence from the SMXL7-mScarlet-I reporter with SMXL5 or SMXL5^{mEAR} after co-expressing AtD14 in *Nbd14a*,*b* is shown. n = 12 leaf discs.

(G) The *in vitro* competitive GST pull-down assay of GST-AtD14 and MBP-SMXL7-GFP in the presence or absence of *rac*-GR24, SMXL5 or SMXL5^{mEAR}. Relative abundance of MBP-SMXL7-GFP was determined by densitometry, with the signal from GST pull-down in the presence of GST-AtD14, MBP-SMXL7-GFP and *rac*-GR24 set as 1.00.

(H) Repression of AtD14-SMXL7 association by SMXL5 or SMXL5^{mEAR} was assessed by split-luciferase complementation assay. n = 12 leaf discs.

(I) Split-luciferase complementation assay for AtD14 interactions with SMXL5 and SMXL5^{mEAR}.

(J) SMXL7 interactions with SMXL5 and SMXL5^{mEAR} were assessed by split-luciferase complementation assay. n = 10-15 leaf discs. Asterisks indicate significant difference using the Student's t test (**p < 0.01).

(K) Yeast two-hybrid assays for SMXL5^{mEAR}-SMXL7 and SMXL5-SMXL7^{mEAR} interactions. 0.5 mM 3-AT was added into -LTH medium to reduce background growth. Serial 10-fold dilutions of yeast cultures starting from OD_{600} 2.5 were spotted onto selective growth medium.

(L) The *in vitro* GST pull-down assay of MBP-SMXL7-GFP and GST-SMXL5 or GST-SMXL5^{mEAR}. Relative abundance of MBP-SMXL7-GFP was determined by densitometry, with the signal from GST pull-down in the presence of GST-SMXL5 and MBP-SMXL7-GFP set as 1.00.

Images in **(B)** and data in **(C)** of wild-type (Col-0); *smxl4*,*5*; and two independent transgenic lines of *pSMXL5*:*SMXL5-YFP smxl4*,*5* are duplicated in Figure **2B** and **2C**, respectively, which were done together in the same experiment.

Box-and-whisker plots in **(A)**, **(C)**, **(H)** and **(I)** with the same letter are not significantly different from one another (Student-Newman-Keuls test, p < 0.05).

Asterisks in **(E)** and **(F)** indicate significant differences to EV control at each time point using the Student's t test (*p < 0.05 and **p < 0.01; ns indicates no significance).

In **(H)**, **(I)** and **(J)**, *N. benthamiana* leaves were transiently co-transformed with *Agrobacterium tumefaciens* strains carrying cLUC, nLUC, or indicated fusions as well as a strain carrying an mCherry transgene as a transformation control. Luminescence was measured without treatment or before and 1 hour after treatment with 10 μM GR24^{5DS}, and was normalized against mCherry fluorescence.

In **(G)** and **(L)**, recombinant proteins were resolved by SDS-PAGE and were visualized via Western blot with anti-GFP antibody. MBP-GFP was used as a control. Panels of GST pull-down and input share the same molecular markers.

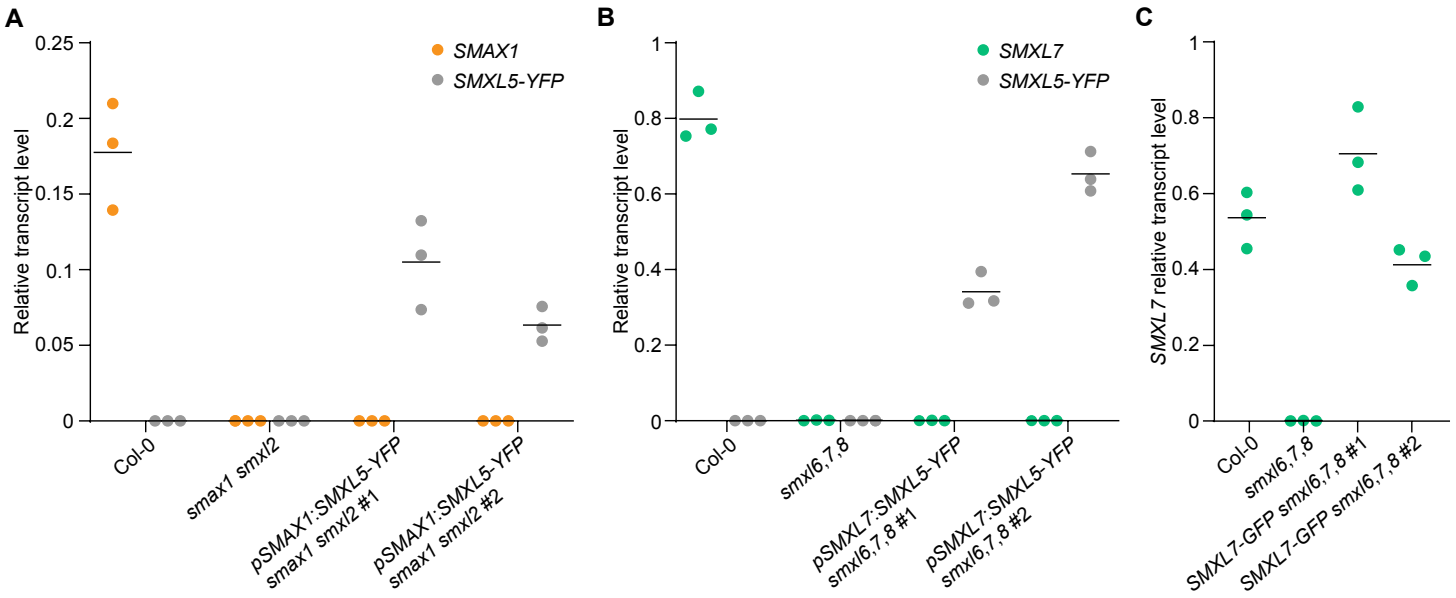

Supplemental Figure 1. Expression of *SMXL* transgenes in Arabidopsis transgenic lines.
(A) RT-qPCR analysis of *SMAX1* and *SMXL5-YFP* transcripts in 7-day-old seedlings of Col-0, *smax1 smxl2* and two independent *pSMAX1*:*SMXL5-YFP smax1 smxl2* transgenic lines.
(B) RT-qPCR analysis of *SMXL7* and *SMXL5-YFP* transcripts in 7-day-old seedlings of Col-0, *smxl6*,*7*,*8* and two independent *pSMXL7*:*SMXL5-YFP smxl6*,*7*,*8* transgenic lines.
(C) RT-qPCR analysis of *SMXL7* transcripts in 7-day-old seedlings of Col-0, *smxl6*,*7*,*8* and two independent *pSMXL7*:*SMXL7-YFP smxl6*,*7*,*8* transgenic lines.
In **(A)**, **(B)** and **(C)**, *SMAX1*, *SMXL7* and *SMXL5-YFP* transcript levels are relative to *CACS* internal reference gene transcripts. Bars indicate the mean. n = 3 pooled tissue samples.

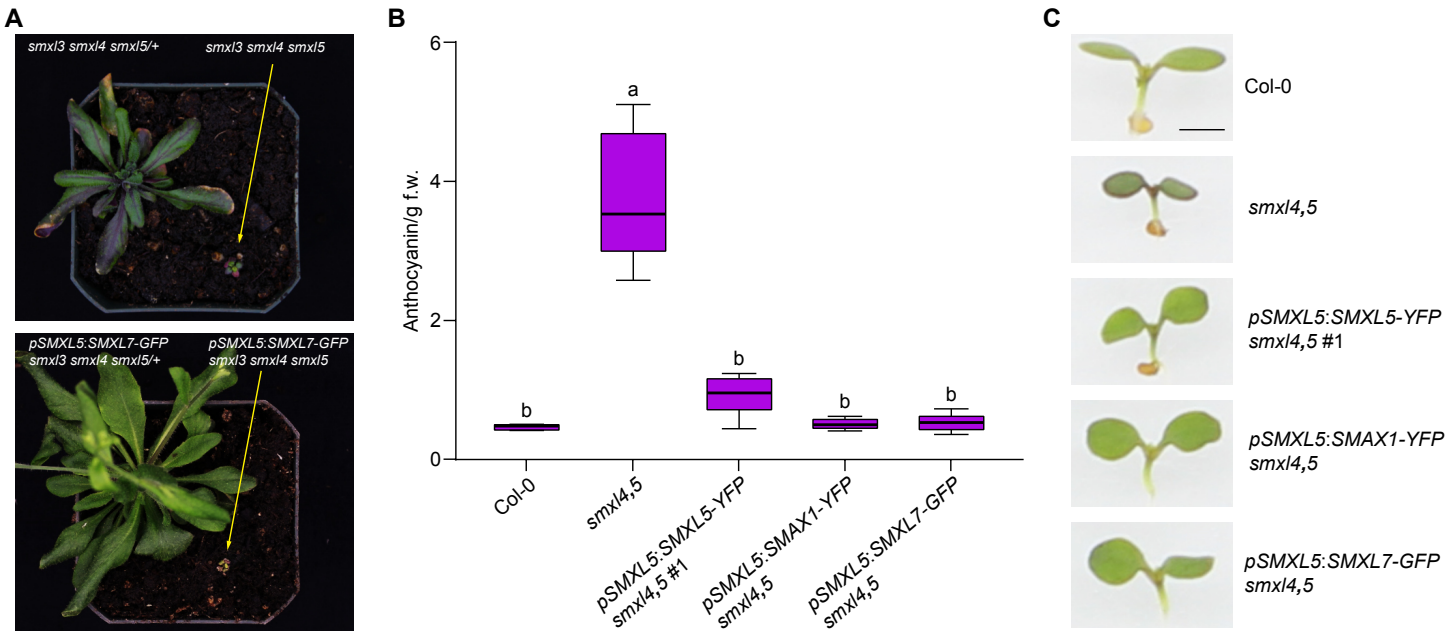

Supplemental Figure 2. *SMXL7* complements *smxl4,5* but not *smxl3,4,5*.

(A) Growth of 4-week-old plants. *smxl3,4,5* and *pSMXL5:SMXL7-GFP smxl3,4,5* are marked by yellow arrows. Bar = 1 cm.

(B) Anthocyanin content in seedlings of wild-type (Col-0), *smxl4,5*, *pSMXL5:SMXL5-YFP smxl4,5* #1, *pSMXL5:SMAX1-YFP smxl4,5* and *pSMXL5:SMXL7-GFP smxl4,5* grown on the 0.5× MS agar with a 16-h-light/8-h-dark photoperiod at 21°C. n = 8 pooled tissue samples. Box-and-whisker plots with the same letter are not significantly different from one another (Student-Newman-Keuls test, $p < 0.05$).

(C) Images of representative 5-day-old seedlings of indicated genotypes in **(B)**. Bar = 1 mm.

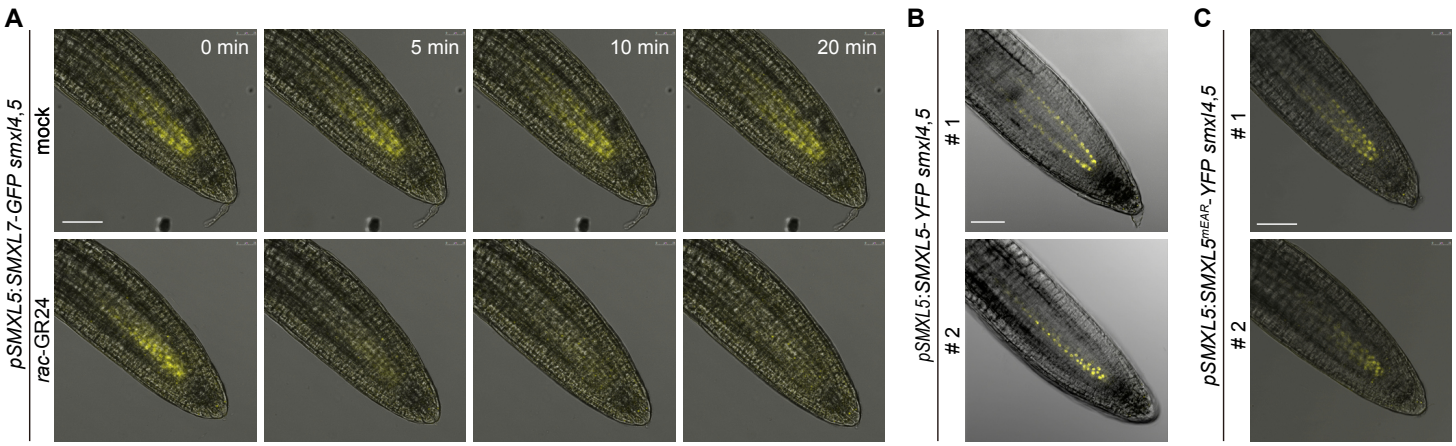

Supplemental Figure 3. Verification of SMXL7-GFP, SMXL5-YFP and SMXL5^{mEAR}-YFP expression driven by *SMXL5* promoter in *smxl4,5*.
5 day-old *smxl4,5* root tips of lines carrying *pSMXL7*:*SMXL5-YFP* **(A)**, *pSMXL5*:*SMXL5-YFP* **(B)** and *pSMXL5*:*SMXL5^{mEAR}-YFP* **(C)** transgenes. Shown are overlaps of bright field (grey) and GFP- or YFP- derived signal (yellow). Treatment of 5 µM *rac*-GR24 or mock was applied in **(A)**. Scale Bars represent 50 µm.

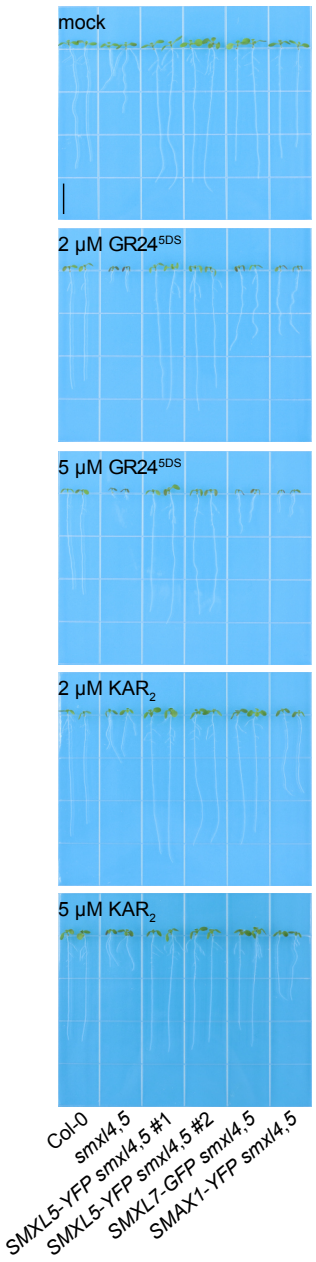

Supplemental Figure 4. Root phenotype of plant materials with GR24^{5DS} or KAR$_2$ treatment in Figure 2A.
Images of representative 9-day-old wild-type (Col-0); *smxl4,5*; two independent transgenic lines of *pSMXL5*:*SMXL5-YFP smxl4,5*; *pSMXL5*:*SMAX1-YFP smxl4,5*; and *pSMXL5*:*SMXL7-GFP smxl4,5* plants grown on 0.5× MS agar containing mock (solvent control) ,2 μM GR24^{5DS}, 5 μM GR24^{5DS}, 2 μM KAR$_2$, or 5 μM KAR$_2$. Bar = 10 mm.

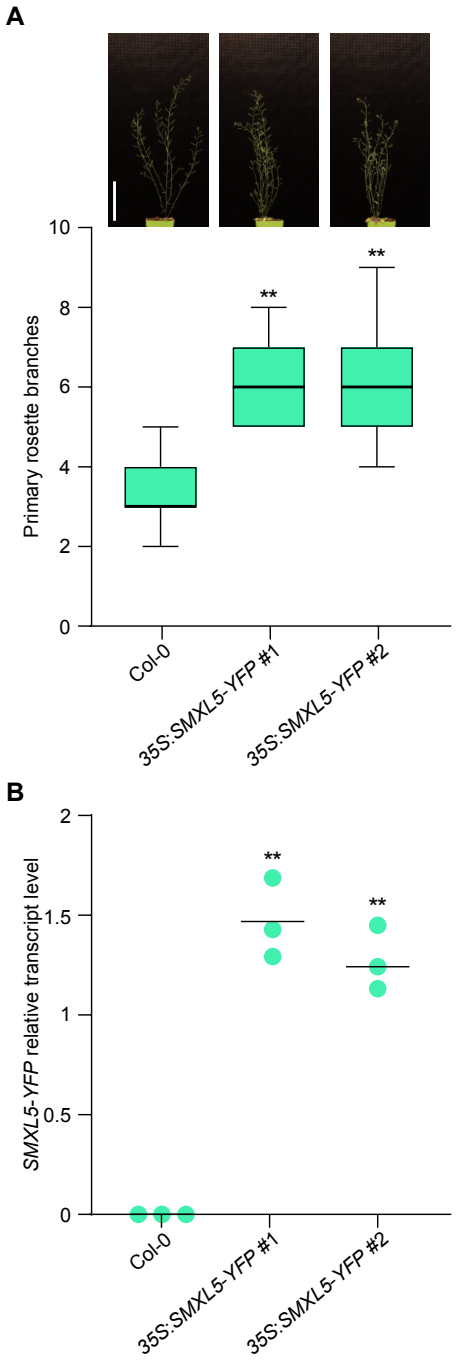

Supplemental Figure 5. Overexpression of *SMXL5* increases primary rosette branch number.

(A) Primary rosette branch number of Col-0 and two independent p*35S*:*SMXL5-YFP* transgenic lines at end of proliferative stage (~7-week-old) grown under white light (~110 µmol m^{-2} s^{-1}) with 16-h-light/8-h-dark photoperiod at 21°C. n = 15. Bar = 10 cm.

(B) RT-qPCR analysis of *SMXL5-YFP* transcripts in 7-day-old seedlings of plant materials in **(A)**. *SMXL5-YFP* transcript level is relative to *CACS* internal reference gene transcripts. Bars indicate the mean. n = 3 pooled tissue samples.

Asterisks in **(A)** and **(B)** indicate significant differences compared with Col-0 using Student's t test (*p < 0.05).

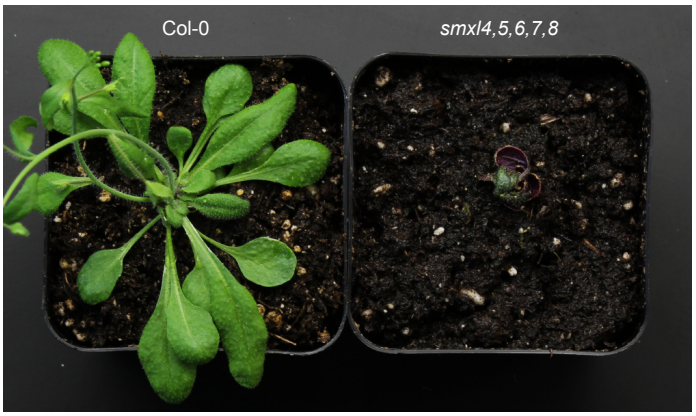

Supplemental Figure 6. Knockout of the *SMXL6/7/8* clade in *smxl4,5* causes severe growth defects and lethality.
Rosette phenotypes of 4-week-old wild-type (Col-0) and *smxl4,5,6,7,8* grown under a long-day photoperiod (16 h light/8 h dark) are shown.

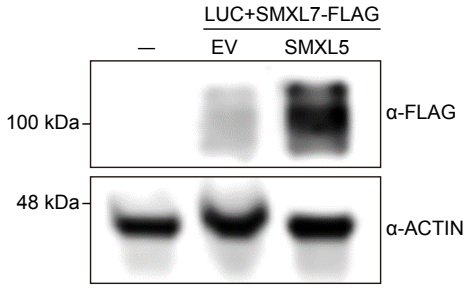

Supplemental Figure 7. Related to Figure 2. SMXL5 enhances SMXL7 stablity to inhibit *BRC1* promoter activity.
Western blot assay to verify SMXL7 level in the presence or absence of SMXL5 in wild-type tobacco leaves in Figure **2G**. *pBRC1*:*LUC* and *35S*:*SMXL7-FLAG* were co-transformed with empty vector (EV) or *35S*:*SMXL5-YFP*. Proteins were detected by immunoblotting with anti-FLAG or anti-ACTIN monoclonal antibody. ACTIN was used as the loading control. Tobacco leaves solely infiltrated with P19 was used as a negative control.

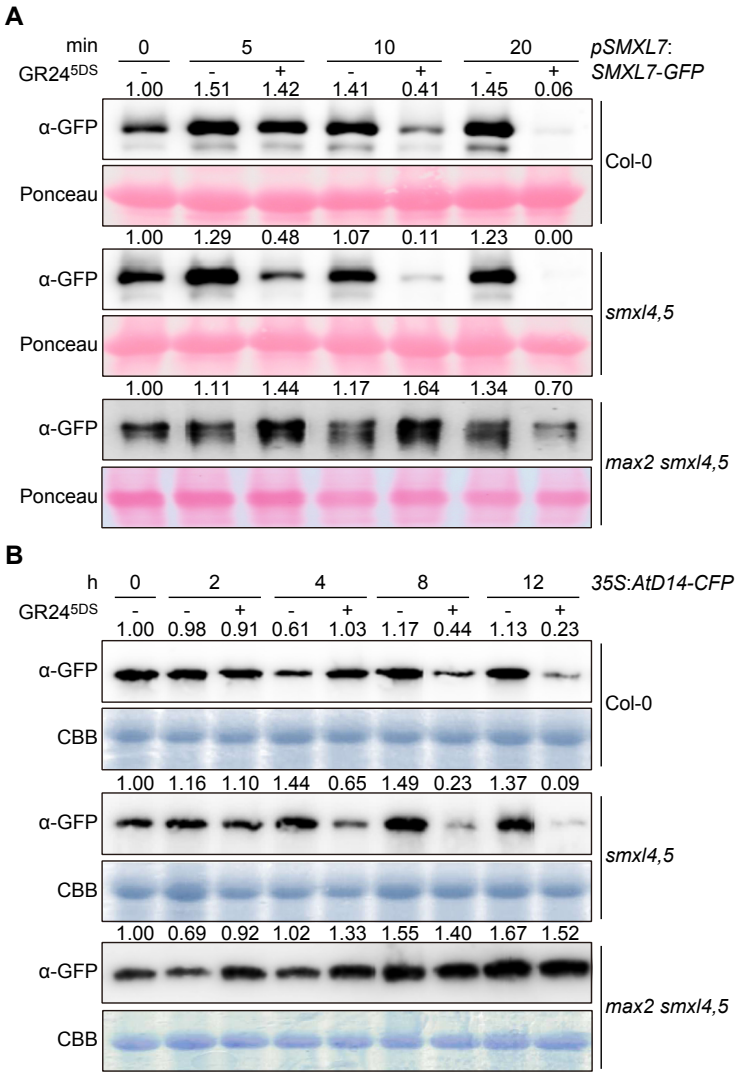

Supplemental Figure 8. Time-course of SMXL7 and D14 levels after GR24^{5DS} treatment in Arabidopsis seedlings.
(A) Degradation of SMXL7-GFP protein in wild-type (Col-0), *smxl4*,*5*, and *max2 smxl4*,*5* Arabidopsis seedlings containing p*SMXL7*:*SMXL7-GFP* transgene. Seedlings were treated for 20 minutes after 7 d of growth with 5 μM GR24^{5DS} in 0.5× MS liquid medium. Ponceau-S stainings of Rubisco are used as the loading control. Proteins were detected by immunoblotting with anti-GFP polyclonal antibody. Relative abundances of SMXL7-GFP was determined by densitometry using ImageJ and normalized to respective loading controls, with the zero-time signal set as 1.00.
(B) Degradation of AtD14-CFP protein in wild-type (Col-0), *smxl4*,*5*, and *max2 smxl4*,*5* Arabidopsis seedlings containing *35S*:*AtD14-CFP* transgene. Seedlings were treated for 12 h after 7 d of growth with 5 μM GR24^{5DS} in 0.5× MS liquid medium. Coomassie brilliant blue (CBB) stainings of Rubisco are used as the loading control. Proteins were detected by immunoblotting with anti-GFP polyclonal antibody. Relative abundances of AtD14-CFP was determined by densitometry using ImageJ and normalized to respective loading controls, with the zero-time signal set as 1.00.

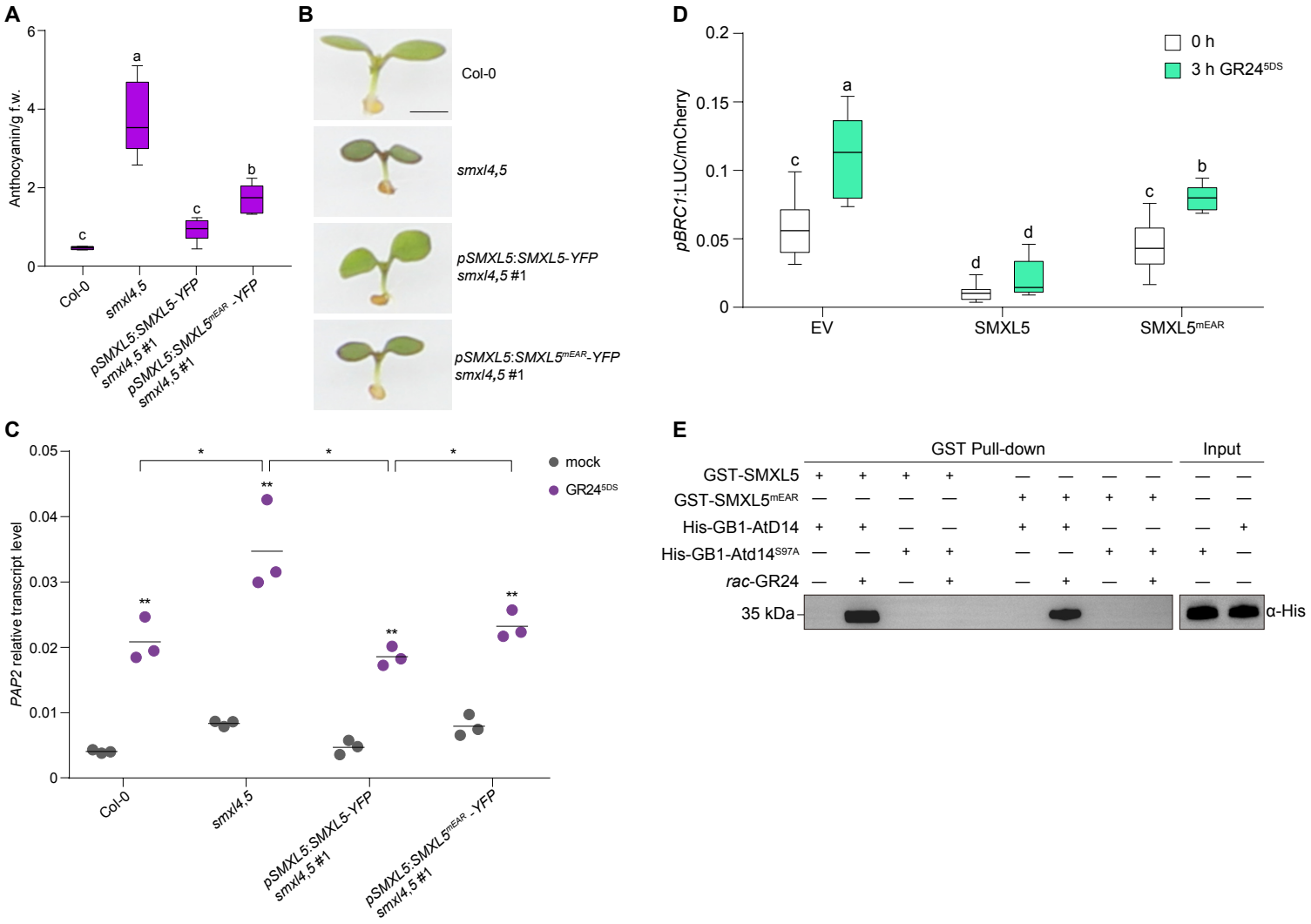

Supplemental Figure 9. The EAR motif is important for SMXL5 functions but not interaction with AtD14.

(A) Anthocyanin accumulation in the 5-day-old seedlings of wild-type (Col-0), *smxl4,5*, *pSMXL5*:*SMXL5-YFP smxl4,5* and *pSMXL5*:*SMXL5*^{mEAR}-*YFP smxl4,5*. n = 8 pooled tissue samples. Box-and-whisker plots with the same letter are not significantly different from one another (Student-Newman-Keuls test, $p < 0.05$).

(B) Images of representative 5-day-old seedlings of indicated genotypes in **(A)**. Bar = 1 mm. Data in **(A)** and images in **(B)** of Col-0, *smxl4,5*, *pSMXL5*:*SMXL5-YFP smxl4,5* are duplicated from Supplemental Figure 2**B** and **C**, respectively, which were done together in the same experiment.

(C) RT-qPCR analysis of *PAP2* gene expression in 7-day-old seedlings of indicated genotypes in **(A)** after 3 h treatment of 5 μM GR24^{5DS} or mock control. *PAP2* transcript level is relative to *CACS* internal reference gene transcripts. Bars indicate the mean. n = 3 pooled tissue samples. Asterisks indicate significant differences to each mock or between compared pairs using Student's t test (*$p < 0.05$ and **$p < 0.01$).

(D) The *pBRC1*:*LUC* reporter activity in the presence of SMXL5 or SMXL5^{mEAR} with the co-expression of SMXL7 in wt tobacco are shown. Leaf discs were treated with 10 μM GR24^{5DS} for 3 h. Luminescence is normalized to mCherry internal control. n = 10 leaf discs. Box-and-whisker plots with the same letter are not significantly different from one another (Student-Newman-Keuls test, $p < 0.05$). Data of EV and SMXL5 is duplicated from Figure **2G**, which was done together in the same experiment.

(E) The *in vitro* GST pull-down of AtD14 and SMXL5 or SMXL5^{mEAR} in the presence or absence of *rac*-GR24. Recombinant proteins were resolved by SDS-PAGE and were visualized via Western blot with anti-His antibody. His-GB1-Atd14^{S97A} with an impaired catalytic triad was used as a negative control. Panels of GST pull-down and input share the same molecular markers. The image of GST pull-down of AtD14 and SMXL5 and the input is duplicated in Figure **6C**.

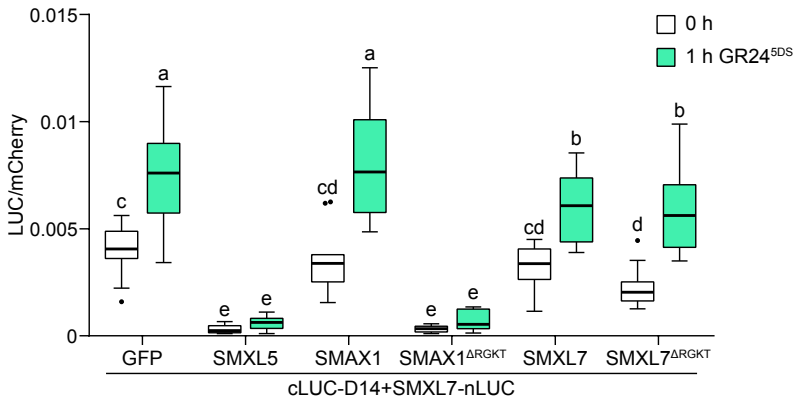

Supplemental Figure 10. SMAX1$^{\Delta RGKT}$ inhibits the interaction of AtD14 and SMXL7.

N. benthamiana leaves were transiently co-transformed with *Agrobacterium tumefaciens* strains carrying cLUC-AtD14, SMXL7-nLUC and indicated fusions as well as a strain carrying an mCherry transgene as a transformation control. *35S*:*GFP*, *35S*:*SMXL5*, *35S*:*SMAX1*, *35S*:*SMAX1*$^{\Delta RGKT}$, *35S*:*SMXL7*, or *35S*:*SMXL7*$^{\Delta RGKT}$ was co-expressed. Luminescence was measured before and 1 hour after treatment with 10 μM GR24^{5DS}, and was normalized against mCherry fluorescence. n = 12 leaf discs. Box-and-whisker plots with the same letter are not significantly different from one another (Student-Newman-Keuls test, $p < 0.05$).